

Measurement of  $e^+e^- \rightarrow \phi\eta'$  cross sections at center-of-mass energies from 3.508 to 4.951 GeV and search for the decay  $\psi(3770) \rightarrow \phi\eta'$

M. Ablikim<sup>1</sup>, M. N. Achasov<sup>5,b</sup>, P. Adlarson<sup>74</sup>, X. C. Ai<sup>80</sup>, R. Aliberti<sup>35</sup>, A. Amoroso<sup>73A,73C</sup>, M. R. An<sup>39</sup>, Q. An<sup>70,57</sup>, Y. Bai<sup>56</sup>, O. Bakina<sup>36</sup>, I. Balossino<sup>29A</sup>, Y. Ban<sup>46,g</sup>, V. Batozskaya<sup>1,44</sup>, K. Begzsuren<sup>32</sup>, N. Berger<sup>35</sup>, M. Berlowski<sup>44</sup>, M. Bertani<sup>28A</sup>, D. Bettoni<sup>29A</sup>, F. Bianchi<sup>73A,73C</sup>, E. Bianco<sup>73A,73C</sup>, A. Bortone<sup>73A,73C</sup>, I. Boyko<sup>36</sup>, R. A. Briere<sup>6</sup>, A. Brueggemann<sup>67</sup>, H. Cai<sup>75</sup>, X. Cai<sup>1,57</sup>, A. Calcaterra<sup>28A</sup>, G. F. Cao<sup>1,62</sup>, N. Cao<sup>1,62</sup>, S. A. Cetin<sup>61A</sup>, J. F. Chang<sup>1,57</sup>, T. T. Chang<sup>76</sup>, W. L. Chang<sup>1,62</sup>, G. R. Che<sup>43</sup>, G. Chelkov<sup>36,a</sup>, C. Chen<sup>43</sup>, Chao Chen<sup>54</sup>, G. Chen<sup>1</sup>, H. S. Chen<sup>1,62</sup>, M. L. Chen<sup>1,57,62</sup>, S. J. Chen<sup>42</sup>, S. M. Chen<sup>60</sup>, T. Chen<sup>1,62</sup>, X. R. Chen<sup>31,62</sup>, X. T. Chen<sup>1,62</sup>, Y. B. Chen<sup>1,57</sup>, Y. Q. Chen<sup>34</sup>, Z. J. Chen<sup>25,h</sup>, W. S. Cheng<sup>73C</sup>, S. K. Choi<sup>11A</sup>, X. Chu<sup>43</sup>, G. Cibinetto<sup>29A</sup>, S. C. Coen<sup>4</sup>, F. Cossio<sup>73C</sup>, J. J. Cui<sup>49</sup>, H. L. Dai<sup>1,57</sup>, J. P. Dai<sup>78</sup>, A. Dbeyssi<sup>18</sup>, R. E. de Boer<sup>4</sup>, D. Dedovich<sup>36</sup>, Z. Y. Deng<sup>1</sup>, A. Denig<sup>35</sup>, I. Denysenko<sup>36</sup>, M. Destefanis<sup>73A,73C</sup>, F. De Mori<sup>73A,73C</sup>, B. Ding<sup>65,1</sup>, X. X. Ding<sup>46,g</sup>, Y. Ding<sup>34</sup>, Y. Ding<sup>40</sup>, J. Dong<sup>1,57</sup>, L. Y. Dong<sup>1,62</sup>, M. Y. Dong<sup>1,57,62</sup>, X. Dong<sup>75</sup>, M. C. Du<sup>1</sup>, S. X. Du<sup>80</sup>, Z. H. Duan<sup>42</sup>, P. Egorov<sup>36,a</sup>, Y. H. Y. Fan<sup>45</sup>, Y. L. Fan<sup>75</sup>, J. Fang<sup>1,57</sup>, S. S. Fang<sup>1,62</sup>, W. X. Fang<sup>1</sup>, Y. Fang<sup>1</sup>, R. Farinelli<sup>29A</sup>, L. Fava<sup>73B,73C</sup>, F. Feldbauer<sup>4</sup>, G. Felici<sup>28A</sup>, C. Q. Feng<sup>70,57</sup>, J. H. Feng<sup>58</sup>, K. Fischer<sup>68</sup>, M. Fritsch<sup>4</sup>, C. Fritsch<sup>67</sup>, C. D. Fu<sup>1</sup>, J. L. Fu<sup>62</sup>, Y. W. Fu<sup>1</sup>, H. Gao<sup>62</sup>, Y. N. Gao<sup>46,g</sup>, Yang Gao<sup>70,57</sup>, S. Garbolino<sup>73C</sup>, I. Garzia<sup>29A,29B</sup>, P. T. Ge<sup>75</sup>, Z. W. Ge<sup>42</sup>, C. Geng<sup>58</sup>, E. M. Gersabeck<sup>66</sup>, A. Gilman<sup>68</sup>, K. Goetzen<sup>14</sup>, L. Gong<sup>40</sup>, W. X. Gong<sup>1,57</sup>, W. Gradl<sup>35</sup>, S. Gramigna<sup>29A,29B</sup>, M. Greco<sup>73A,73C</sup>, M. H. Gu<sup>1,57</sup>, C. Y. Guan<sup>1,62</sup>, Z. L. Guan<sup>22</sup>, A. Q. Guo<sup>31,62</sup>, L. B. Guo<sup>41</sup>, M. J. Guo<sup>49</sup>, R. P. Guo<sup>48</sup>, Y. P. Guo<sup>13,f</sup>, A. Guskov<sup>36,a</sup>, T. T. Han<sup>49</sup>, W. Y. Han<sup>39</sup>, X. Q. Hao<sup>19</sup>, F. A. Harris<sup>64</sup>, K. K. He<sup>54</sup>, K. L. He<sup>1,62</sup>, F. H. Heinsius<sup>4</sup>, C. H. Heinz<sup>35</sup>, Y. K. Heng<sup>1,57,62</sup>, C. Herold<sup>59</sup>, T. Holtmann<sup>4</sup>, P. C. Hong<sup>13,f</sup>, G. Y. Hou<sup>1,62</sup>, X. T. Hou<sup>1,62</sup>, Y. R. Hou<sup>62</sup>, Z. L. Hou<sup>1</sup>, H. M. Hu<sup>1,62</sup>, J. F. Hu<sup>55,i</sup>, T. Hu<sup>1,57,62</sup>, Y. Hu<sup>1</sup>, G. S. Huang<sup>70,57</sup>, K. X. Huang<sup>58</sup>, L. Q. Huang<sup>31,62</sup>, X. T. Huang<sup>49</sup>, Y. P. Huang<sup>1</sup>, T. Hussain<sup>72</sup>, N. Hüskens<sup>27,35</sup>, W. Imoehl<sup>27</sup>, N. in der Wiesche<sup>67</sup>, J. Jackson<sup>27</sup>, S. Jaeger<sup>4</sup>, S. Janchiv<sup>32</sup>, J. H. Jeong<sup>11A</sup>, Q. Ji<sup>1</sup>, Q. P. Ji<sup>19</sup>, X. B. Ji<sup>1,62</sup>, X. L. Ji<sup>1,57</sup>, Y. Y. Ji<sup>49</sup>, X. Q. Jia<sup>49</sup>, Z. K. Jia<sup>70,57</sup>, H. J. Jiang<sup>75</sup>, P. C. Jiang<sup>46,g</sup>, S. S. Jiang<sup>39</sup>, T. J. Jiang<sup>16</sup>, X. S. Jiang<sup>1,57,62</sup>, Y. Jiang<sup>62</sup>, J. B. Jiao<sup>49</sup>, Z. Jiao<sup>23</sup>, S. Jin<sup>42</sup>, Y. Jin<sup>65</sup>, M. Q. Jing<sup>1,62</sup>, T. Johansson<sup>74</sup>, X. K.<sup>1</sup>, S. Kabana<sup>33</sup>, N. Kalantar-Nayestanaki<sup>63</sup>, X. L. Kang<sup>10</sup>, X. S. Kang<sup>40</sup>, M. Kavatsyuk<sup>63</sup>, B. C. Ke<sup>80</sup>, A. Khoukaz<sup>67</sup>, R. Kiuchi<sup>1</sup>, R. Klient<sup>14</sup>, O. B. Kolcu<sup>61A</sup>, B. Kopf<sup>4</sup>, M. Kuessner<sup>4</sup>, A. Kupsc<sup>44,74</sup>, W. Kühn<sup>37</sup>, J. J. Lane<sup>66</sup>, P. Larin<sup>18</sup>, A. Lavanaia<sup>26</sup>, L. Lavezzi<sup>73A,73C</sup>, T. T. Lei<sup>70,57</sup>, Z. H. Lei<sup>70,57</sup>, H. Leithoff<sup>35</sup>, M. Lellmann<sup>35</sup>, T. Lenz<sup>35</sup>, C. Li<sup>43</sup>, C. Li<sup>47</sup>, C. H. Li<sup>39</sup>, Cheng Li<sup>70,57</sup>, D. M. Li<sup>80</sup>, F. Li<sup>1,57</sup>, G. Li<sup>1</sup>, H. Li<sup>70,57</sup>, H. B. Li<sup>1,62</sup>, H. J. Li<sup>19</sup>, H. N. Li<sup>55,i</sup>, Hui Li<sup>43</sup>, J. R. Li<sup>60</sup>, J. S. Li<sup>58</sup>, J. W. Li<sup>49</sup>, K. L. Li<sup>19</sup>, Ke Li<sup>1</sup>, L. J. Li<sup>1,62</sup>, L. K. Li<sup>1</sup>, Lei Li<sup>3</sup>, M. H. Li<sup>43</sup>, P. R. Li<sup>38,j,k</sup>, Q. X. Li<sup>49</sup>, S. X. Li<sup>13</sup>, T. Li<sup>49</sup>, W. D. Li<sup>1,62</sup>, W. G. Li<sup>1</sup>, X. H. Li<sup>70,57</sup>, X. L. Li<sup>49</sup>, Xiaoyu Li<sup>1,62</sup>, Y. G. Li<sup>46,g</sup>, Z. J. Li<sup>58</sup>, C. Liang<sup>42</sup>, H. Liang<sup>1,62</sup>, H. Liang<sup>70,57</sup>, H. Liang<sup>34</sup>, Y. F. Liang<sup>53</sup>, Y. T. Liang<sup>31,62</sup>, G. R. Liao<sup>15</sup>, L. Z. Liao<sup>49</sup>, Y. P. Liao<sup>1,62</sup>, J. Libby<sup>26</sup>, A. Limphirat<sup>59</sup>, D. X. Lin<sup>31,62</sup>, T. Lin<sup>1</sup>, B. J. Liu<sup>1</sup>, B. X. Liu<sup>75</sup>, C. Liu<sup>34</sup>, C. X. Liu<sup>1</sup>, F. H. Liu<sup>52</sup>, Fang Liu<sup>1</sup>, Feng Liu<sup>7</sup>, G. M. Liu<sup>55,i</sup>, H. Liu<sup>38,j,k</sup>, H. M. Liu<sup>1,62</sup>, Huanhuan Liu<sup>1</sup>, Huihui Liu<sup>21</sup>, J. B. Liu<sup>70,57</sup>, J. L. Liu<sup>71</sup>, J. Y. Liu<sup>1,62</sup>, K. Liu<sup>1</sup>, K. Y. Liu<sup>40</sup>, Ke Liu<sup>22</sup>, L. Liu<sup>70,57</sup>, L. C. Liu<sup>43</sup>, Lu Liu<sup>43</sup>, M. H. Liu<sup>13,f</sup>, P. L. Liu<sup>1</sup>, Q. Liu<sup>62</sup>, S. B. Liu<sup>70,57</sup>, T. Liu<sup>13,f</sup>, W. K. Liu<sup>43</sup>, W. M. Liu<sup>70,57</sup>, X. Liu<sup>38,j,k</sup>, Y. Liu<sup>38,j,k</sup>, Y. Liu<sup>80</sup>, Y. B. Liu<sup>43</sup>, Z. A. Liu<sup>1,57,62</sup>, Z. Q. Liu<sup>49</sup>, X. C. Lou<sup>1,57,62</sup>, F. X. Lu<sup>58</sup>, H. J. Lu<sup>23</sup>, J. G. Lu<sup>1,57</sup>, X. L. Lu<sup>1</sup>, Y. Lu<sup>8</sup>, Y. P. Lu<sup>1,57</sup>, Z. H. Lu<sup>1,62</sup>, C. L. Luo<sup>41</sup>, M. X. Luo<sup>79</sup>, T. Luo<sup>13,f</sup>, X. L. Luo<sup>1,57</sup>, X. R. Lyu<sup>62</sup>, Y. F. Lyu<sup>43</sup>, F. C. Ma<sup>40</sup>, H. L. Ma<sup>1</sup>, J. L. Ma<sup>1,62</sup>, L. L. Ma<sup>49</sup>, M. M. Ma<sup>1,62</sup>, Q. M. Ma<sup>1</sup>, R. Q. Ma<sup>1,62</sup>, R. T. Ma<sup>62</sup>, X. Y. Ma<sup>1,57</sup>, Y. Ma<sup>46,g</sup>, Y. M. Ma<sup>31</sup>, F. E. Maas<sup>18</sup>, M. Maggiora<sup>73A,73C</sup>, S. Malde<sup>68</sup>, Q. A. Malik<sup>72</sup>, A. Mangoni<sup>28B</sup>, Y. J. Mao<sup>46,g</sup>, Z. P. Mao<sup>1</sup>, S. Marcello<sup>73A,73C</sup>, Z. X. Meng<sup>65</sup>, J. G. Messchendorp<sup>14,63</sup>, G. Mezzadri<sup>29A</sup>, H. Miao<sup>1,62</sup>, T. J. Min<sup>42</sup>, R. E. Mitchell<sup>27</sup>, X. H. Mo<sup>1,57,62</sup>, N. Yu. Muchnoi<sup>5,b</sup>, J. Muskalla<sup>35</sup>, Y. Nefedov<sup>36</sup>, F. Nerling<sup>18,d</sup>, I. B. Nikolaev<sup>5,b</sup>, Z. Ning<sup>1,57</sup>, S. Nisar<sup>12,l</sup>, W. D. Niu<sup>54</sup>, Y. Niu<sup>49</sup>, S. L. Olsen<sup>62</sup>, Q. Ouyang<sup>1,57,62</sup>, S. Pacetti<sup>28B,28C</sup>, X. Pan<sup>54</sup>, Y. Pan<sup>56</sup>, A. Pathak<sup>34</sup>, P. Patteri<sup>28A</sup>, Y. P. Pei<sup>70,57</sup>, M. Pelizaeus<sup>4</sup>, H. P. Peng<sup>70,57</sup>, K. Peters<sup>14,d</sup>, J. L. Ping<sup>41</sup>, R. G. Ping<sup>1,62</sup>, S. Plura<sup>35</sup>, S. Pogodin<sup>36</sup>, V. Prasad<sup>33</sup>, F. Z. Qi<sup>1</sup>, H. Qi<sup>70,57</sup>, H. R. Qi<sup>60</sup>, M. Qi<sup>42</sup>, T. Y. Qi<sup>13,f</sup>, S. Qian<sup>1,57</sup>, W. B. Qian<sup>62</sup>, C. F. Qiao<sup>62</sup>, J. J. Qin<sup>71</sup>, L. Q. Qin<sup>15</sup>, X. P. Qin<sup>13,f</sup>, X. S. Qin<sup>49</sup>, Z. H. Qin<sup>1,57</sup>, J. F. Qiu<sup>1</sup>, S. Q. Qu<sup>60</sup>, C. F. Redmer<sup>35</sup>, K. J. Ren<sup>39</sup>, A. Rivetti<sup>73C</sup>, M. Rolo<sup>73C</sup>, G. Rong<sup>1,62</sup>, Ch. Rosner<sup>18</sup>, S. N. Ruan<sup>43</sup>, N. Salone<sup>44</sup>, A. Sarantsev<sup>36,c</sup>, Y. Schelhaas<sup>35</sup>, K. Schoenning<sup>74</sup>, M. Scodreggio<sup>29A,29B</sup>, K. Y. Shan<sup>13,f</sup>, W. Shan<sup>24</sup>, X. Y. Shan<sup>70,57</sup>, J. F. Shanguan<sup>54</sup>, L. G. Shao<sup>1,62</sup>, M. Shao<sup>70,57</sup>, C. P. Shen<sup>13,f</sup>, H. F. Shen<sup>1,62</sup>, W. H. Shen<sup>62</sup>, X. Y. Shen<sup>1,62</sup>, B. A. Shi<sup>62</sup>, H. C. Shi<sup>70,57</sup>, J. L. Shi<sup>13</sup>, J. Y. Shi<sup>1</sup>, Q. Q. Shi<sup>54</sup>, R. S. Shi<sup>1,62</sup>, X. Shi<sup>1,57</sup>, J. J. Song<sup>19</sup>, T. Z. Song<sup>58</sup>, W. M. Song<sup>34,1</sup>, Y. J. Song<sup>13</sup>, Y. X. Song<sup>46,g</sup>, S. Sosio<sup>73A,73C</sup>, S. Spataro<sup>73A,73C</sup>, F. Stieler<sup>35</sup>, Y. J. Su<sup>62</sup>, G. B. Sun<sup>75</sup>, G. X. Sun<sup>1</sup>, H. Sun<sup>62</sup>, H. K. Sun<sup>1</sup>, J. F. Sun<sup>19</sup>, K. Sun<sup>60</sup>,

L. Sun<sup>75</sup>, S. S. Sun<sup>1,62</sup>, T. Sun<sup>1,62</sup>, W. Y. Sun<sup>34</sup>, Y. Sun<sup>10</sup>, Y. J. Sun<sup>70,57</sup>, Y. Z. Sun<sup>1</sup>, Z. T. Sun<sup>49</sup>, Y. X. Tan<sup>70,57</sup>,  
 C. J. Tang<sup>53</sup>, G. Y. Tang<sup>1</sup>, J. Tang<sup>58</sup>, Y. A. Tang<sup>75</sup>, L. Y. Tao<sup>71</sup>, Q. T. Tao<sup>25,h</sup>, M. Tat<sup>68</sup>, J. X. Teng<sup>70,57</sup>,  
 V. Thoren<sup>74</sup>, W. H. Tian<sup>51</sup>, W. H. Tian<sup>58</sup>, Y. Tian<sup>31,62</sup>, Z. F. Tian<sup>75</sup>, I. Uman<sup>61B</sup>, S. J. Wang<sup>49</sup>, B. Wang<sup>1</sup>,  
 B. L. Wang<sup>62</sup>, Bo Wang<sup>70,57</sup>, C. W. Wang<sup>42</sup>, D. Y. Wang<sup>46,g</sup>, F. Wang<sup>71</sup>, H. J. Wang<sup>38,j,k</sup>, H. P. Wang<sup>1,62</sup>,  
 J. P. Wang<sup>49</sup>, K. Wang<sup>1,57</sup>, L. L. Wang<sup>1</sup>, M. Wang<sup>49</sup>, Meng Wang<sup>1,62</sup>, S. Wang<sup>38,j,k</sup>, S. Wang<sup>13,f</sup>, T. Wang<sup>13,f</sup>,  
 T. J. Wang<sup>43</sup>, W. Wang<sup>71</sup>, W. Wang<sup>58</sup>, W. P. Wang<sup>70,57</sup>, X. Wang<sup>46,g</sup>, X. F. Wang<sup>38,j,k</sup>, X. J. Wang<sup>39</sup>,  
 X. L. Wang<sup>13,f</sup>, Y. Wang<sup>60</sup>, Y. D. Wang<sup>45</sup>, Y. F. Wang<sup>1,57,62</sup>, Y. H. Wang<sup>47</sup>, Y. N. Wang<sup>45</sup>, Y. Q. Wang<sup>1</sup>,  
 Yaqian Wang<sup>17,1</sup>, Yi Wang<sup>60</sup>, Z. Wang<sup>1,57</sup>, Z. L. Wang<sup>71</sup>, Z. Y. Wang<sup>1,62</sup>, Ziyi Wang<sup>62</sup>, D. Wei<sup>69</sup>, D. H. Wei<sup>15</sup>,  
 F. Weidner<sup>67</sup>, S. P. Wen<sup>1</sup>, C. W. Wenzel<sup>4</sup>, U. Wiedner<sup>4</sup>, G. Wilkinson<sup>68</sup>, M. Wolke<sup>74</sup>, L. Wollenberg<sup>4</sup>, C. Wu<sup>39</sup>,  
 J. F. Wu<sup>1,62</sup>, L. H. Wu<sup>1</sup>, L. J. Wu<sup>1,62</sup>, X. Wu<sup>13,f</sup>, X. H. Wu<sup>34</sup>, Y. Wu<sup>70</sup>, Y. H. Wu<sup>54</sup>, Y. J. Wu<sup>31</sup>, Z. Wu<sup>1,57</sup>,  
 L. Xia<sup>70,57</sup>, X. M. Xian<sup>39</sup>, T. Xiang<sup>46,g</sup>, D. Xiao<sup>38,j,k</sup>, G. Y. Xiao<sup>42</sup>, S. Y. Xiao<sup>1</sup>, Y. L. Xiao<sup>13,f</sup>, Z. J. Xiao<sup>41</sup>,  
 C. Xie<sup>42</sup>, X. H. Xie<sup>46,g</sup>, Y. Xie<sup>49</sup>, Y. G. Xie<sup>1,57</sup>, Y. H. Xie<sup>7</sup>, Z. P. Xie<sup>70,57</sup>, T. Y. Xing<sup>1,62</sup>, C. F. Xu<sup>1,62</sup>,  
 C. J. Xu<sup>58</sup>, G. F. Xu<sup>1</sup>, H. Y. Xu<sup>65</sup>, Q. J. Xu<sup>16</sup>, Q. N. Xu<sup>30</sup>, W. Xu<sup>1,62</sup>, W. L. Xu<sup>65</sup>, X. P. Xu<sup>54</sup>, Y. C. Xu<sup>77</sup>,  
 Z. P. Xu<sup>42</sup>, Z. S. Xu<sup>62</sup>, F. Yan<sup>13,f</sup>, L. Yan<sup>13,f</sup>, W. B. Yan<sup>70,57</sup>, W. C. Yan<sup>80</sup>, X. Q. Yan<sup>1</sup>, H. J. Yang<sup>50,e</sup>,  
 H. L. Yang<sup>34</sup>, H. X. Yang<sup>1</sup>, Tao Yang<sup>1</sup>, Y. Yang<sup>13,f</sup>, Y. F. Yang<sup>43</sup>, Y. X. Yang<sup>1,62</sup>, Yifan Yang<sup>1,62</sup>, Z. W. Yang<sup>38,j,k</sup>,  
 Z. P. Yao<sup>49</sup>, M. Ye<sup>1,57</sup>, M. H. Ye<sup>9</sup>, J. H. Yin<sup>1</sup>, Z. Y. You<sup>58</sup>, B. X. Yu<sup>1,57,62</sup>, C. X. Yu<sup>43</sup>, G. Yu<sup>1,62</sup>, J. S. Yu<sup>25,h</sup>,  
 T. Yu<sup>71</sup>, X. D. Yu<sup>46,g</sup>, C. Z. Yuan<sup>1,62</sup>, L. Yuan<sup>2</sup>, S. C. Yuan<sup>1</sup>, X. Q. Yuan<sup>1</sup>, Y. Yuan<sup>1,62</sup>, Z. Y. Yuan<sup>58</sup>,  
 C. X. Yue<sup>39</sup>, A. A. Zafar<sup>72</sup>, F. R. Zeng<sup>49</sup>, X. Zeng<sup>13,f</sup>, Y. Zeng<sup>25,h</sup>, Y. J. Zeng<sup>1,62</sup>, X. Y. Zhai<sup>34</sup>, Y. C. Zhai<sup>49</sup>,  
 Y. H. Zhan<sup>58</sup>, A. Q. Zhang<sup>1,62</sup>, B. L. Zhang<sup>1,62</sup>, B. X. Zhang<sup>1</sup>, D. H. Zhang<sup>43</sup>, G. Y. Zhang<sup>19</sup>, H. Zhang<sup>70</sup>,  
 H. H. Zhang<sup>58</sup>, H. H. Zhang<sup>34</sup>, H. Q. Zhang<sup>1,57,62</sup>, H. Y. Zhang<sup>1,57</sup>, J. Zhang<sup>80</sup>, J. J. Zhang<sup>51</sup>, J. L. Zhang<sup>20</sup>,  
 J. Q. Zhang<sup>41</sup>, J. W. Zhang<sup>1,57,62</sup>, J. X. Zhang<sup>38,j,k</sup>, J. Y. Zhang<sup>1</sup>, J. Z. Zhang<sup>1,62</sup>, Jianyu Zhang<sup>62</sup>,  
 Jiawei Zhang<sup>1,62</sup>, L. M. Zhang<sup>60</sup>, L. Q. Zhang<sup>58</sup>, Lei Zhang<sup>42</sup>, P. Zhang<sup>1,62</sup>, Q. Y. Zhang<sup>39,80</sup>, Shuihan Zhang<sup>1,62</sup>,  
 Shulei Zhang<sup>25,h</sup>, X. D. Zhang<sup>45</sup>, X. M. Zhang<sup>1</sup>, X. Y. Zhang<sup>49</sup>, Xuyan Zhang<sup>54</sup>, Y. Zhang<sup>68</sup>, Y. Zhang<sup>71</sup>, Y.  
 T. Zhang<sup>80</sup>, Y. H. Zhang<sup>1,57</sup>, Yan Zhang<sup>70,57</sup>, Yao Zhang<sup>1</sup>, Z. H. Zhang<sup>1</sup>, Z. L. Zhang<sup>34</sup>, Z. Y. Zhang<sup>75</sup>,  
 Z. Y. Zhang<sup>43</sup>, G. Zhao<sup>1</sup>, J. Zhao<sup>39</sup>, J. Y. Zhao<sup>1,62</sup>, J. Z. Zhao<sup>1,57</sup>, Lei Zhao<sup>70,57</sup>, Ling Zhao<sup>1</sup>, M. G. Zhao<sup>43</sup>,  
 S. J. Zhao<sup>80</sup>, Y. B. Zhao<sup>1,57</sup>, Y. X. Zhao<sup>31,62</sup>, Z. G. Zhao<sup>70,57</sup>, A. Zhemchugov<sup>36,a</sup>, B. Zheng<sup>71</sup>, J. P. Zheng<sup>1,57</sup>,  
 W. J. Zheng<sup>1,62</sup>, Y. H. Zheng<sup>62</sup>, B. Zhong<sup>41</sup>, X. Zhong<sup>58</sup>, H. Zhou<sup>49</sup>, L. P. Zhou<sup>1,62</sup>, X. Zhou<sup>75</sup>, X. K. Zhou<sup>7</sup>,  
 X. R. Zhou<sup>70,57</sup>, X. Y. Zhou<sup>39</sup>, Y. Z. Zhou<sup>13,f</sup>, J. Zhu<sup>43</sup>, K. Zhu<sup>1</sup>, K. J. Zhu<sup>1,57,62</sup>, L. Zhu<sup>34</sup>, L. X. Zhu<sup>62</sup>,  
 S. H. Zhu<sup>69</sup>, S. Q. Zhu<sup>42</sup>, T. J. Zhu<sup>13,f</sup>, W. J. Zhu<sup>13,f</sup>, Y. C. Zhu<sup>70,57</sup>, Z. A. Zhu<sup>1,62</sup>, J. H. Zou<sup>1</sup>, J. Zu<sup>70,57</sup>

(BESIII Collaboration)

<sup>1</sup> *Institute of High Energy Physics, Beijing 100049, People's Republic of China*

<sup>2</sup> *Beihang University, Beijing 100191, People's Republic of China*

<sup>3</sup> *Beijing Institute of Petrochemical Technology, Beijing 102617, People's Republic of China*

<sup>4</sup> *Bochum Ruhr-University, D-44780 Bochum, Germany*

<sup>5</sup> *Budker Institute of Nuclear Physics SB RAS (BINP), Novosibirsk 630090, Russia*

<sup>6</sup> *Carnegie Mellon University, Pittsburgh, Pennsylvania 15213, USA*

<sup>7</sup> *Central China Normal University, Wuhan 430079, People's Republic of China*

<sup>8</sup> *Central South University, Changsha 410083, People's Republic of China*

<sup>9</sup> *China Center of Advanced Science and Technology, Beijing 100190, People's Republic of China*

<sup>10</sup> *China University of Geosciences, Wuhan 430074, People's Republic of China*

<sup>11</sup> *Chung-Ang University, Seoul, 06974, Republic of Korea*

<sup>12</sup> *COMSATS University Islamabad, Lahore Campus, Defence Road, Off Raiwind Road, 54000 Lahore, Pakistan*

<sup>13</sup> *Fudan University, Shanghai 200433, People's Republic of China*

<sup>14</sup> *GSI Helmholtzcentre for Heavy Ion Research GmbH, D-64291 Darmstadt, Germany*

<sup>15</sup> *Guangxi Normal University, Guilin 541004, People's Republic of China*

<sup>16</sup> *Hangzhou Normal University, Hangzhou 310036, People's Republic of China*

<sup>17</sup> *Hebei University, Baoding 071002, People's Republic of China*

<sup>18</sup> *Helmholtz Institute Mainz, Staudinger Weg 18, D-55099 Mainz, Germany*

<sup>19</sup> *Henan Normal University, Xinxiang 453007, People's Republic of China*

<sup>20</sup> *Henan University, Kaifeng 475004, People's Republic of China*

<sup>21</sup> *Henan University of Science and Technology, Luoyang 471003, People's Republic of China*

<sup>22</sup> *Henan University of Technology, Zhengzhou 450001, People's Republic of China*

<sup>23</sup> *Huangshan College, Huangshan 245000, People's Republic of China*

- <sup>24</sup> Hunan Normal University, Changsha 410081, People's Republic of China
- <sup>25</sup> Hunan University, Changsha 410082, People's Republic of China
- <sup>26</sup> Indian Institute of Technology Madras, Chennai 600036, India
- <sup>27</sup> Indiana University, Bloomington, Indiana 47405, USA
- <sup>28</sup> INFN Laboratori Nazionali di Frascati, (A)INFN Laboratori Nazionali di Frascati, I-00044, Frascati, Italy; (B)INFN Sezione di Perugia, I-06100, Perugia, Italy; (C)University of Perugia, I-06100, Perugia, Italy
- <sup>29</sup> INFN Sezione di Ferrara, (A)INFN Sezione di Ferrara, I-44122, Ferrara, Italy; (B)University of Ferrara, I-44122, Ferrara, Italy
- <sup>30</sup> Inner Mongolia University, Hohhot 010021, People's Republic of China
- <sup>31</sup> Institute of Modern Physics, Lanzhou 730000, People's Republic of China
- <sup>32</sup> Institute of Physics and Technology, Peace Avenue 54B, Ulaanbaatar 13330, Mongolia
- <sup>33</sup> Instituto de Alta Investigación, Universidad de Tarapacá, Casilla 7D, Arica 1000000, Chile
- <sup>34</sup> Jilin University, Changchun 130012, People's Republic of China
- <sup>35</sup> Johannes Gutenberg University of Mainz, Johann-Joachim-Becher-Weg 45, D-55099 Mainz, Germany
- <sup>36</sup> Joint Institute for Nuclear Research, 141980 Dubna, Moscow region, Russia
- <sup>37</sup> Justus-Liebig-Universität Giessen, II. Physikalisches Institut, Heinrich-Buff-Ring 16, D-35392 Giessen, Germany
- <sup>38</sup> Lanzhou University, Lanzhou 730000, People's Republic of China
- <sup>39</sup> Liaoning Normal University, Dalian 116029, People's Republic of China
- <sup>40</sup> Liaoning University, Shenyang 110036, People's Republic of China
- <sup>41</sup> Nanjing Normal University, Nanjing 210023, People's Republic of China
- <sup>42</sup> Nanjing University, Nanjing 210093, People's Republic of China
- <sup>43</sup> Nankai University, Tianjin 300071, People's Republic of China
- <sup>44</sup> National Centre for Nuclear Research, Warsaw 02-093, Poland
- <sup>45</sup> North China Electric Power University, Beijing 102206, People's Republic of China
- <sup>46</sup> Peking University, Beijing 100871, People's Republic of China
- <sup>47</sup> Qufu Normal University, Qufu 273165, People's Republic of China
- <sup>48</sup> Shandong Normal University, Jinan 250014, People's Republic of China
- <sup>49</sup> Shandong University, Jinan 250100, People's Republic of China
- <sup>50</sup> Shanghai Jiao Tong University, Shanghai 200240, People's Republic of China
- <sup>51</sup> Shanxi Normal University, Linfen 041004, People's Republic of China
- <sup>52</sup> Shanxi University, Taiyuan 030006, People's Republic of China
- <sup>53</sup> Sichuan University, Chengdu 610064, People's Republic of China
- <sup>54</sup> Soochow University, Suzhou 215006, People's Republic of China
- <sup>55</sup> South China Normal University, Guangzhou 510006, People's Republic of China
- <sup>56</sup> Southeast University, Nanjing 211100, People's Republic of China
- <sup>57</sup> State Key Laboratory of Particle Detection and Electronics, Beijing 100049, Hefei 230026, People's Republic of China
- <sup>58</sup> Sun Yat-Sen University, Guangzhou 510275, People's Republic of China
- <sup>59</sup> Suranaree University of Technology, University Avenue 111, Nakhon Ratchasima 30000, Thailand
- <sup>60</sup> Tsinghua University, Beijing 100084, People's Republic of China
- <sup>61</sup> Turkish Accelerator Center Particle Factory Group, (A)Istinye University, 34010, Istanbul, Turkey; (B)Near East University, Nicosia, North Cyprus, 99138, Mersin 10, Turkey
- <sup>62</sup> University of Chinese Academy of Sciences, Beijing 100049, People's Republic of China
- <sup>63</sup> University of Groningen, NL-9747 AA Groningen, The Netherlands
- <sup>64</sup> University of Hawaii, Honolulu, Hawaii 96822, USA
- <sup>65</sup> University of Jinan, Jinan 250022, People's Republic of China
- <sup>66</sup> University of Manchester, Oxford Road, Manchester, M13 9PL, United Kingdom
- <sup>67</sup> University of Muenster, Wilhelm-Klemm-Strasse 9, 48149 Muenster, Germany
- <sup>68</sup> University of Oxford, Keble Road, Oxford OX13RH, United Kingdom
- <sup>69</sup> University of Science and Technology Liaoning, Anshan 114051, People's Republic of China
- <sup>70</sup> University of Science and Technology of China, Hefei 230026, People's Republic of China
- <sup>71</sup> University of South China, Hengyang 421001, People's Republic of China
- <sup>72</sup> University of the Punjab, Lahore-54590, Pakistan

<sup>73</sup> *University of Turin and INFN, (A)University of Turin, I-10125, Turin, Italy; (B)University of Eastern Piedmont, I-15121, Alessandria, Italy; (C)INFN, I-10125, Turin, Italy*

<sup>74</sup> *Uppsala University, Box 516, SE-75120 Uppsala, Sweden*

<sup>75</sup> *Wuhan University, Wuhan 430072, People's Republic of China*

<sup>76</sup> *Xinyang Normal University, Xinyang 464000, People's Republic of China*

<sup>77</sup> *Yantai University, Yantai 264005, People's Republic of China*

<sup>78</sup> *Yunnan University, Kunming 650500, People's Republic of China*

<sup>79</sup> *Zhejiang University, Hangzhou 310027, People's Republic of China*

<sup>80</sup> *Zhengzhou University, Zhengzhou 450001, People's Republic of China*

<sup>a</sup> *Also at the Moscow Institute of Physics and Technology, Moscow 141700, Russia*

<sup>b</sup> *Also at the Novosibirsk State University, Novosibirsk, 630090, Russia*

<sup>c</sup> *Also at the NRC "Kurchatov Institute", PNPI, 188300, Gatchina, Russia*

<sup>d</sup> *Also at Goethe University Frankfurt, 60323 Frankfurt am Main, Germany*

<sup>e</sup> *Also at Key Laboratory for Particle Physics, Astrophysics and Cosmology, Ministry of Education; Shanghai Key Laboratory for Particle Physics and Cosmology; Institute of Nuclear and Particle Physics, Shanghai 200240, People's Republic of China*

<sup>f</sup> *Also at Key Laboratory of Nuclear Physics and Ion-beam Application (MOE) and Institute of Modern Physics, Fudan University, Shanghai 200443, People's Republic of China*

<sup>g</sup> *Also at State Key Laboratory of Nuclear Physics and Technology, Peking University, Beijing 100871, People's Republic of China*

<sup>h</sup> *Also at School of Physics and Electronics, Hunan University, Changsha 410082, China*

<sup>i</sup> *Also at Guangdong Provincial Key Laboratory of Nuclear Science, Institute of Quantum Matter, South China Normal University, Guangzhou 510006, China*

<sup>j</sup> *Also at Frontiers Science Center for Rare Isotopes, Lanzhou University, Lanzhou 730000, People's Republic of China*

<sup>k</sup> *Also at Lanzhou Center for Theoretical Physics, Lanzhou University, Lanzhou 730000, People's Republic of China*

<sup>l</sup> *Also at the Department of Mathematical Sciences, IBA, Karachi 75270, Pakistan*

(Dated: September 12, 2023)

The cross sections of the  $e^+e^- \rightarrow \phi\eta'$  process at center-of-mass energies from 3.508 to 4.951 GeV are measured with high precision using 26.1 fb<sup>-1</sup> data collected with the BESIII detector operating at the BEPCII storage ring. The cross sections are of the order of a few picobarn, and decrease as the center-of-mass energy increases as  $s^{-n/2}$  with  $n = 4.35 \pm 0.14$ . This result is in agreement with the Nambu-Jona-Lasinio model prediction of  $n = 3.5 \pm 0.9$ . In addition, the charmless decay  $\psi(3770) \rightarrow \phi\eta'$  is searched for by fitting the measured cross sections, yet no significant signal is observed. The upper limit of  $\mathcal{B}(\psi(3770) \rightarrow \phi\eta')$  at the 90% confidence level is determined to be  $2.3 \times 10^{-5}$ .

## I. INTRODUCTION

The study of  $e^+e^-$  annihilation into light hadrons is essential to understand the production mechanism of light hadrons and reveal fundamental aspects of the strong interactions of light quarks [1]. Within the chiral perturbation framework, the Nambu-Jona-Lasinio (NJL) model has been successful in describing the dynamics of strong interactions between elementary particles and predicting the cross sections of the  $e^+e^- \rightarrow$  vector meson + pseudoscalar meson (VP) process over a range of center-of-mass (c.m.) energies ( $\sqrt{s}$ ) from 2.3 to 5.5 GeV [2–5], here we only refer to the light hadrons final states. Within large experimental uncertainties, the cross sections of the  $e^+e^- \rightarrow \rho\eta'$  process measured by the BABAR Collaboration [6] are consistent with the NJL model predictions [7]. The NJL model also predicts that the cross sections of the  $e^+e^- \rightarrow \phi\eta'$  process from  $\sqrt{s}=3.5$  to

5.0 GeV are expected to be  $\sim 60$  picobarn and follow an asymptotic power-law behavior of  $\sigma \propto s^{-n/2}$  with  $n = 3.5 \pm 0.9$  as can be derived from the result in [7]. However, these predictions have never been tested with high-precision experimental data.

The  $\psi(3770)$ , observed in the 1970s [8], is the first charmonium resonance above the  $D\bar{D}$  production threshold. It is expected to decay almost entirely to Okubo-Zweig-Iizuka-allowed  $D\bar{D}$  final states while the fractions of hadronic and radiative transitions to lower lying charmonium states and decays into light hadrons (states with  $u, d, s$  quarks) are predicted to be small [9, 10]. Unexpectedly, the BES experiment measured a branching fraction for  $\psi(3770) \rightarrow$  non- $D\bar{D}$  to be  $(14.7 \pm 3.2)\%$  [11–14], while the CLEO result is  $(-3.3 \pm 1.4^{+6.6}_{-4.8})\%$  [15]. Taking the charmonium transition into account [16–20], a few percent of  $\psi(3770)$  decays into light hadrons are still allowed due to the large width of  $\psi(3770)$ . Although

BES, CLEO-c, and BESIII searched for exclusive  $\psi(3770)$  decays into light hadrons, no significant signal for any decay was reported [21, 22]. Until now, the sum of the branching fractions of the known non- $D\bar{D}$  decays of the  $\psi(3770)$  remains to be less than 2% [23]. Recently, BESIII measured the branching fraction for the inclusive decay  $\psi(3770) \rightarrow J/\psi X$ , which are consistent within error with the sum of published branching fractions ( $0.47 \pm 0.06$ )% [23], of  $\psi(3770) \rightarrow \pi^+\pi^-J/\psi, \pi^0\pi^0J/\psi, \eta J/\psi$ , and  $\gamma\chi_{cJ}$  with  $J = 0, 1, 2$  [24].

Although the  $\psi(3770)$  is believed to be primarily the  $1^3D_1$  state of the  $c\bar{c}$  system, its large leptonic width of ( $0.262 \pm 0.018$ ) keV indicates substantial mixing with the  $S$ -wave state [25, 26]. The  $S$ - and  $D$ -wave mixing scheme has been used to explain the “ $\rho\pi$  puzzle” in  $\psi(2S)$  and  $J/\psi$  decays [27, 28] and may suggest that the small branching fractions for  $\psi(2S) \rightarrow VP$  decays can be enhanced in  $\psi(3770) \rightarrow VP$  decays, including  $\rho\pi$ ,  $\phi\eta$ ,  $\phi\eta'$ , and so on. Analogous to the observed charmless decay of  $\psi(3770) \rightarrow \phi\eta$  [21], we search for the related decay  $\psi(3770) \rightarrow \phi\eta'$ . By using the known branching fractions of  $J/\psi \rightarrow \phi\eta'$  and  $\psi(2S) \rightarrow \phi\eta'$  [23], and taking into account the mixing angle  $\theta$  between  $S$ - and  $D$ -wave, the  $\psi(3770) \rightarrow \phi\eta'$  decay branching fraction ( $\mathcal{B}_{\phi\eta'}$ ) is predicted to be  $(0.46 \pm 0.18) \times 10^{-5} < \mathcal{B}_{\phi\eta'} < (3.5 \pm 1.3) \times 10^{-5}$  [29, 30]. This decay can be searched for with the BESIII data at the  $\psi(3770)$  peak and in its vicinity.

A recent BESIII paper [31] reported a study of the  $e^+e^- \rightarrow \phi\eta'$  process and a search for the charmless decay  $Y(4230) \rightarrow \phi\eta'$  with part of the data used in this analysis. In this article, we report a measurement of the cross sections of the  $e^+e^- \rightarrow \phi\eta'$  process with  $26.1 \text{ fb}^{-1}$  data collected at  $\sqrt{s} = 3.508 \sim 4.951 \text{ GeV}$  [32] to test the NJL model prediction and to search for the charmless decay  $\psi(3770) \rightarrow \phi\eta'$ . Due to the low integrated luminosity of the  $\psi(3770)$  scan data samples, we do not use the  $\psi(3770)$  scan presented in the BESIII work [24].

## II. DETECTOR AND DATA SAMPLES

The BESIII detector [32] records symmetric  $e^+e^-$  collisions provided by the BEPCII storage ring [33] in the  $\sqrt{s}$  range from 2.0 to 4.95 GeV, with a peak luminosity of  $1.05 \times 10^{33} \text{ cm}^{-2}\text{s}^{-1}$  achieved at  $\sqrt{s} = 3.77 \text{ GeV}$ . The cylindrical core of BESIII detector consists of a helium-based multilayer drift chamber (MDC), a plastic scintillator time-of-flight system (TOF), and a CsI (TI) electromagnetic calorimeter (EMC), which are all enclosed in a superconducting solenoidal magnet providing a 1.0 T magnetic field [34]. The solenoid is supported by an octagonal flux-return yoke with resistive plate counter muon identifier modules interleaved with steel. The acceptance of charged particles and photons is 93% over  $4\pi$  solid angle. The charged particle momentum resolution at 1 GeV/ $c$  is 0.5%, and the specific ionization

energy loss  $dE/dx$  resolution is 6% for the electrons from Bhabha scattering. The EMC measures photon energies with a resolution of 2.5% (5%) at 1 GeV in the barrel (end cap) region. The time resolution of the TOF barrel part is 68 ps, while that of the end cap part is 110 ps. The end cap TOF system was upgraded in 2015 with multi-gap resistive plate chamber technology, providing a time resolution of 60 ps [35, 36].

Details of the data samples used in this analysis are listed in Table I. The optimization of event selection criteria and efficiency determination are based on Monte Carlo (MC) simulations. The GEANT4-based [37] simulation software, BESIII Object Oriented Simulation Tool (BOOST) [38], includes the geometric description of the BESIII detectors. The beam energy spread and initial state radiation (ISR) in the  $e^+e^-$  annihilation are modeled with the generator KKMC [39, 40].

Samples of MC events for the signal process  $e^+e^- \rightarrow \phi\eta'$  are generated using the HELAMP model within the EVTGEN framework [41, 42], which allow simulations of any two-body decay by specifying the helicity amplitudes for the final state particles. The subsequent decay  $\phi \rightarrow K^+K^-$  is generated with the Vector-Scalar-Scalar (VSS) model in which a vector particle decays into two scalars. The angular distribution of  $K$  is proportional to  $\sin^2\theta_K$  in the  $\phi$  helicity frame [41], where  $\theta_K$  is the helicity angle of  $K$  in  $\phi$  helicity frame. The decay  $\eta' \rightarrow \gamma\pi^+\pi^-$  is generated with the DIY generator taking into account both  $\rho-\omega$  interference and the box anomaly [43]. The decays  $\eta' \rightarrow \eta\pi^+\pi^-$  and  $\eta \rightarrow \gamma\gamma$  are both generated uniformly in phase space. Final state radiation associated with charged final state particles is handled by PHOTOS [44].

The inclusive MC samples generated at  $\sqrt{s}=3.650, 3.773, 4.178, 4.416, \text{ and } 4.843 \text{ GeV}$  are used to estimate the possible background. The continuum processes are incorporated in KKMC, and the QED processes such as Bhabha scattering,  $\mu^+\mu^-$ ,  $\tau^+\tau^-$ , and  $\gamma\gamma$  events are generated with KKMC and BABAYAGA [45]. All particle decays are modelled with EVTGEN using branching fractions either taken from the Particle Data Group (PDG) [23], when available, or otherwise estimated with LUNDCHARM for  $J/\psi$  and  $\psi(2S)$  decays [46, 47].

## III. EVENT SELECTION

Charged tracks detected in the MDC are required to be within a polar angle ( $\theta$ ) range of  $|\cos\theta| < 0.93$ , where  $\theta$  is defined with respect to the  $z$ -axis, the symmetry axis of the MDC. For charged tracks, the distances of the closest approach to the interaction point along the  $z$ -axis and in the transverse plane must be less than 10 cm and 1 cm, respectively. Photon candidates are identified using showers in the EMC. The deposited energy of each shower must be more than 25 MeV in the barrel

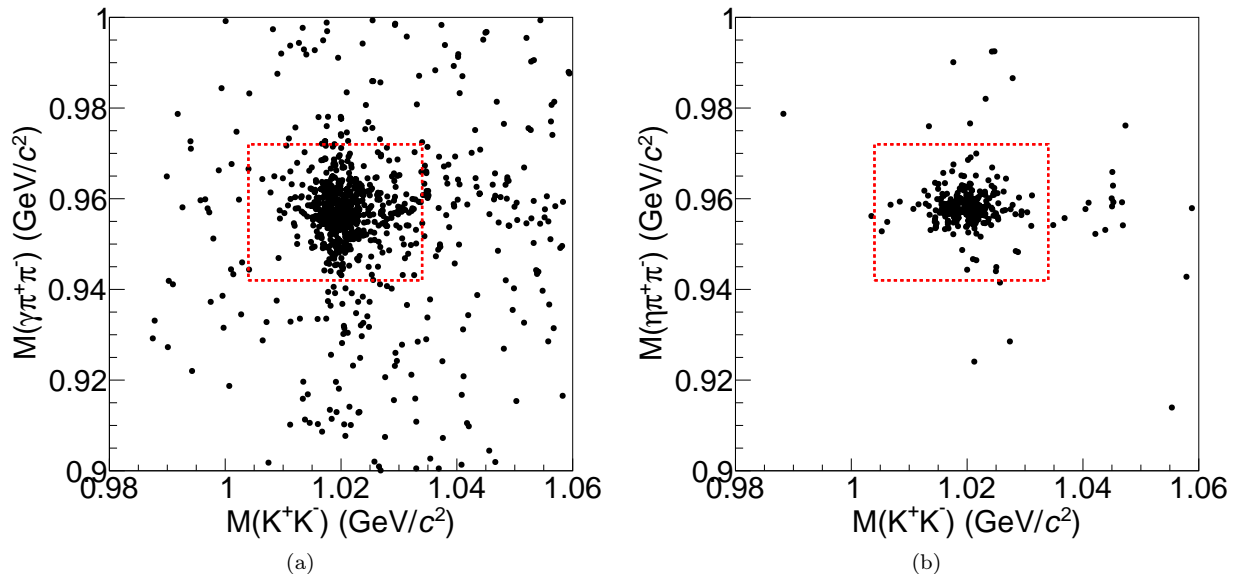


Fig. 1. The two-dimensional distribution of  $M(K^+K^-)$  versus  $M(\gamma\pi^+\pi^-)$  for mode I (a) and versus  $M(\eta\pi^+\pi^-)$  for mode II (b) from data at  $\sqrt{s}=3.773$  GeV. The red rectangle indicates the signal region.

region ( $|\cos\theta| < 0.80$ ) and more than 50 MeV in the end cap region ( $0.86 < |\cos\theta| < 0.92$ ). To significantly reduce showers that originate from charged tracks, the angle subtended by the EMC shower and the position of the closest charged track at the EMC must be greater than 10 degrees as measured from the interaction point. To suppress electronic noise and showers unrelated to the event, the difference between the EMC time and the event start time is required to be within  $[0, 700]$  ns. To reconstruct  $e^+e^- \rightarrow \phi\eta'$ , the  $\phi$  candidate is reconstructed via the  $K^+K^-$  decays, and the  $\eta'$  candidate is reconstructed via  $\gamma\pi^+\pi^-$  (mode I) and  $\eta\pi^+\pi^-$  with  $\eta \rightarrow \gamma\gamma$  (mode II). We require exactly four charged tracks with zero net-charge and at least one (two) photon(s) candidates in an event for mode I (II). A vertex fit is performed on the four charged tracks to ensure they originate from the same vertex. In order to select  $\phi$  candidates, for both modes I and II, we test all possible combinations of oppositely charged particles which are assumed to be kaons. A  $\phi$  candidate is selected if it satisfies  $|M(K^+K^-) - m_\phi| < 0.04$  GeV/ $c^2$  ( $M(K^+K^-)$  is the invariant mass of  $K^+K^-$  and  $m_\phi$  is the nominal mass of  $\phi$  from PDG [23]). To remove a combinatorial background, events with more than one selected  $\phi$  candidate are rejected. According to the MC simulation, this reduces the signal statistics by about 1%. A four-constraint (4C) kinematic fit, which constrains the sum of four momentum of the final-state particles to the four momentum of the initial colliding beams, is performed for the final state particles of mode I in each event to improve resolutions and suppress the background. If there is more than one combination due to multiple photons in an event, the one with the smallest  $\chi_{4C}^2$  is selected. The  $\chi_{4C}^2$  is required to be less than 100 for mode I. For

mode II, a five-constraint (5C) kinematic fit is performed with an additional constraint to the invariant mass of the  $\eta$  candidate to the  $\eta$  nominal mass from PDG [23]. We loop over all possible combinations of  $\eta$  candidates and select the one with the least  $\chi_{5C}^2$  of the kinematic fit. The  $\chi_{5C}^2$  is required to be less than 200 for mode II. All the selection criteria have been optimized by maximizing the figure of merit  $S/\sqrt{S+B}$ , where  $S(B)$  is the number of signal (background) events in the signal region, determined by MC simulation. The signal candidates for  $\phi$  and  $\eta'$  mesons are required to be within the mass ranges  $1.004 \leq M(K^+K^-) \leq 1.034$  GeV/ $c^2$  for both modes, and  $0.943 \leq M(\gamma(\eta)\pi^+\pi^-) \leq 0.973$  GeV/ $c^2$  for mode I (II).

After applying the mentioned selection criteria, Fig. 1 shows the scatter plots of  $M(K^+K^-)$  versus  $M(\gamma\pi^+\pi^-)$  and  $M(\eta\pi^+\pi^-)$  in data at  $\sqrt{s}=3.773$  GeV for modes I and II. Two clear accumulations of signal are observed in Fig. 1 around the intersection of the  $\phi$  and  $\eta'$  signal regions. We have used the sidebands of  $\phi$  and  $\eta'$  in data to check the possible peaking backgrounds from  $K^+K^-\eta'$  and  $\gamma(\eta)\pi^+\pi^-\phi$ , and we do not observe obvious peaking backgrounds.

To extract the signal yield, an unbinned maximum likelihood fit is performed on the  $M(\gamma\pi^+\pi^-)$  and  $M(\eta\pi^+\pi^-)$  distributions for modes I and II, respectively. In the fit, the signal is described by the line shape of the  $\eta'$  from MC simulation convolved with a Gaussian function, which accounts for the difference in resolutions between data and MC simulation, and the background is described by a linear function. The parameters of the Gaussian function and the linear function are free in the fit. Due to the low statistics at  $\sqrt{s}=3.670, 3.867, 3.871, 4.278, 4.308, 4.467, 4.527, 4.699, 4.740, 4.918,$  and  $4.951$  GeV, the pa-

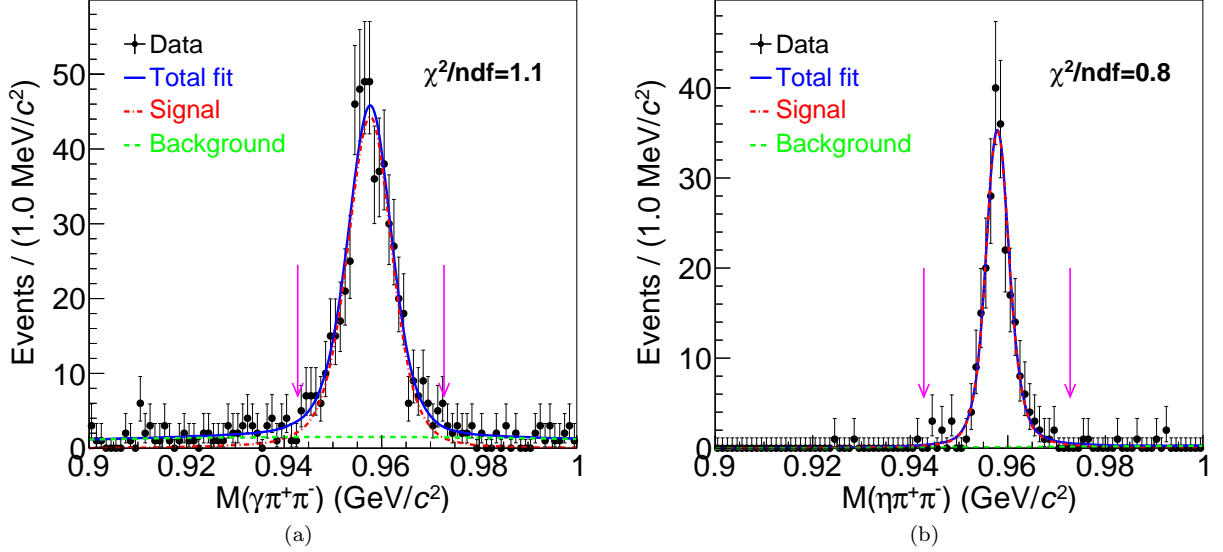


Fig. 2. The unbinned maximum likelihood fits on the distributions of  $M(\gamma\pi^+\pi^-)$  for mode I (a) and  $M(\eta\pi^+\pi^-)$  for mode II (b) at  $\sqrt{s}=3.773$  GeV. The black dots with error bars represent the data sample, the red dot-dashed lines represent the signal MC sample, the green dashed lines are the fitted background and the blue solid lines represent the total fit. The signal region lies between the two pink solid arrows.

parameters of the Gaussian function are fixed to the values obtained from the nearby data samples with large statistics for mode I. For mode II, the background level is very low and the parameters of the Gaussian function are free in the fit. The fit results at  $\sqrt{s}=3.773$  GeV for modes I and II are shown in Fig. 2. The results for the number of events within the signal region,  $N_i^{\text{signal}}$ , are obtained from the fits for all data samples and listed in Table I. The uncertainty of  $N_i^{\text{signal}}$  obtained from the fit may be smaller than  $\sqrt{N_i^{\text{signal}}}$ , because the fit range is larger than the signal region. The uncertainty of  $N_i^{\text{signal}}$  is estimated with MINOS in TMINUIT [48].

#### IV. CROSS SECTION MEASUREMENT OF THE $e^+e^- \rightarrow \phi\eta'$ PROCESS

The dressed cross section of the  $e^+e^- \rightarrow \phi\eta'$  process at each energy point is calculated with

$$\sigma_i^{\text{dressed}} = \frac{\sigma_i^{\text{Born}}}{|1-\Pi|^2} = \frac{N_i^{\text{signal}}}{\mathcal{L} \cdot (1+\delta) \cdot \epsilon_i \cdot \mathcal{B}_i}, \quad (1)$$

where  $\sigma_i^{\text{Born}}$  is the Born cross section,  $N_i^{\text{signal}}$  is the number of signal events extracted from the fit to the  $M(\gamma\pi^+\pi^-)$  or  $M(\eta\pi^+\pi^-)$  distribution as described in Sec. III,  $\mathcal{L}$  is the integrated luminosity,  $\epsilon_i$  is the selection efficiency obtained from the MC simulation, and  $\mathcal{B}_i$  is the product of the branching fractions  $\mathcal{B}(\phi \rightarrow K^+K^-) \cdot \mathcal{B}(\eta' \rightarrow \gamma\pi^+\pi^-)$  or  $\mathcal{B}(\phi \rightarrow K^+K^-) \cdot \mathcal{B}(\eta' \rightarrow \eta\pi^+\pi^-) \cdot \mathcal{B}(\eta \rightarrow \gamma\gamma)$ , taken from PDG [23]. The subscript

$i$  represents mode I or mode II. The vacuum polarization factor  $\frac{1}{|1-\Pi|^2}$  is taken from Ref. [49], and the radiative correction factor  $(1+\delta)$  is defined as

$$(1+\delta) = \frac{\sigma_i^{\text{obs}}}{\sigma_i^{\text{dressed}}} = \frac{\int \sigma_i^{\text{dressed}}(s(1-x))F(x,s)dx}{\sigma_i^{\text{dressed}}(s)}, \quad (2)$$

where  $F(x,s)$  is the QED radiator function with an accuracy of 0.1% [50],  $x = 2E_\gamma/\sqrt{s}$  the scaled ISR photon energy, and  $\sigma_i^{\text{obs}} = N_i^{\text{signal}}/(\mathcal{L} \cdot \epsilon_i \cdot \mathcal{B}_i)$  the observed cross section.

The cross sections we get from each of the modes are compatible with each other, and the combined dressed cross section of these two modes is calculated with

$$\sigma_{\text{com}}^{\text{dressed}} = \frac{N_{\text{com}}^{\text{signal}}}{\mathcal{L} \cdot (1+\delta) \cdot \sum_i \epsilon_i \cdot \mathcal{B}_i}, \quad (3)$$

where  $N_{\text{com}}^{\text{signal}}$  is the total number of signal events in the two modes. To get more accurate ISR factors, an iterative procedure is used [51]. The results of the cross sections are summarized in Table I and shown in Fig. 3. We can see that the cross sections range between 0.7 and 7.5 pb and decrease gradually as  $\sqrt{s}$  increases. There is no visible structure from the contribution of a vector charmonium or a charmonium-like state in this energy region.

Least-chi-square fits to the measured dressed cross sections are performed to describe the continuum line shape and to search for the  $\psi(3770) \rightarrow \phi\eta'$  decay. The  $\chi^2$  is

Table I. Signal yields and cross sections for the  $e^+e^- \rightarrow \phi\eta'$  process at different c.m. energies ( $\sqrt{s}$ ) [52–54]. Here,  $\mathcal{L}$ ,  $N^{\text{signal}}$ ,  $\epsilon$ ,  $(1 + \delta)$ , and  $\frac{1}{|1-\Pi|^2}$  are the integrated luminosity [53–55], the number of signal events in the signal region, the detection efficiency, the radiative correction factor, and the vacuum polarization factor, respectively.  $\sigma_{\text{com}}^{\text{dressed}}$  and  $\sigma_{\text{com}}^{\text{Born}}$  are the combined dressed cross section and Born cross section of the  $e^+e^- \rightarrow \phi\eta'$  process, where the first uncertainties are statistical, and the second uncertainties are systematic. The subscripts I and II represent modes I and II, respectively.

$\sqrt{s}$ (GeV)	$\mathcal{L}$ (pb $^{-1}$ )	$N_I^{\text{signal}}$	$N_{II}^{\text{signal}}$	$\epsilon_I$ (%)	$\epsilon_{II}$ (%)	$(1 + \delta)$	$\frac{1}{ 1-\Pi ^2}$	$\sigma_{\text{com}}^{\text{dressed}}$ (pb)	$\sigma_{\text{com}}^{\text{Born}}$ (pb)
3.508	181.8	46.1 $^{+7.3}_{-7.3}$	15.6 $^{+4.3}_{-3.6}$	32.52%	25.79%	0.734	1.044	6.75 $^{+0.93}_{-0.89}$ ±0.34	6.47 $^{+0.89}_{-0.85}$ ±0.32
3.511	184.6	50.3 $^{+7.5}_{-7.5}$	22.4 $^{+5.4}_{-4.7}$	32.47%	26.02%	0.737	1.044	7.79 $^{+0.99}_{-0.95}$ ±0.39	7.46 $^{+0.95}_{-0.91}$ ±0.37
3.582	85.7	25.0 $^{+5.2}_{-5.2}$	7.5 $^{+3.1}_{-2.5}$	31.09%	25.02%	0.792	1.039	7.28 $^{+1.36}_{-1.29}$ ±0.36	7.01 $^{+1.31}_{-1.24}$ ±0.35
3.650	453.9	94.0 $^{+10.4}_{-10.4}$	37.5 $^{+6.7}_{-6.0}$	30.48%	24.23%	0.915	1.021	4.93 $^{+0.46}_{-0.45}$ ±0.25	4.83 $^{+0.45}_{-0.44}$ ±0.24
3.670	84.7	13.2 $^{+3.6}_{-3.6}$	6.8 $^{+2.9}_{-2.2}$	30.12%	24.20%	0.839	0.994	4.42 $^{+1.02}_{-0.93}$ ±0.22	4.45 $^{+1.03}_{-0.94}$ ±0.24
3.773	2931.8	538.8 $^{+24.9}_{-24.9}$	237.0 $^{+15.6}_{-15.6}$	28.33%	22.28%	0.960	1.056	4.63 $^{+0.18}_{-0.18}$ ±0.23	4.39 $^{+0.17}_{-0.17}$ ±0.22
3.808	50.5	7.4 $^{+3.2}_{-2.6}$	2.9 $^{+2.0}_{-1.4}$	30.09%	23.88%	0.896	1.056	3.59 $^{+1.32}_{-1.03}$ ±0.18	3.40 $^{+1.25}_{-0.98}$ ±0.17
3.867	108.9	8.8 $^{+3.7}_{-3.1}$	6.8 $^{+3.1}_{-2.5}$	29.26%	23.45%	0.918	1.051	2.53 $^{+0.78}_{-0.64}$ ±0.13	2.40 $^{+0.74}_{-0.61}$ ±0.12
3.871	110.3	19.9 $^{+4.6}_{-4.6}$	5.8 $^{+2.7}_{-2.1}$	29.29%	23.17%	0.919	1.051	4.12 $^{+0.85}_{-0.81}$ ±0.21	3.92 $^{+0.81}_{-0.77}$ ±0.20
3.896	52.6	11.0 $^{+3.8}_{-3.2}$	3.9 $^{+2.3}_{-1.6}$	29.44%	23.61%	0.927	1.049	4.91 $^{+1.46}_{-1.18}$ ±0.25	4.68 $^{+1.40}_{-1.12}$ ±0.23
4.008	482.0	52.5 $^{+7.9}_{-7.9}$	30.4 $^{+6.0}_{-5.4}$	28.52%	22.79%	0.964	1.044	2.96 $^{+0.35}_{-0.34}$ ±0.15	2.84 $^{+0.34}_{-0.33}$ ±0.14
4.085	52.9	7.1 $^{+3.1}_{-2.5}$	2.0 $^{+1.7}_{-1.1}$	28.34%	22.61%	0.988	1.051	2.91 $^{+1.13}_{-0.87}$ ±0.15	2.77 $^{+1.08}_{-0.83}$ ±0.14
4.128	401.5	37.4 $^{+6.5}_{-6.5}$	21.4 $^{+4.9}_{-4.2}$	27.66%	21.95%	1.047	1.052	2.40 $^{+0.33}_{-0.32}$ ±0.12	2.28 $^{+0.32}_{-0.30}$ ±0.11
4.157	408.7	41.3 $^{+6.8}_{-6.8}$	9.2 $^{+3.6}_{-2.9}$	27.75%	22.26%	1.052	1.053	2.00 $^{+0.31}_{-0.29}$ ±0.10	1.90 $^{+0.29}_{-0.28}$ ±0.10
4.178	3189.0	299.1 $^{+17.9}_{-17.9}$	113.6 $^{+11.1}_{-10.4}$	27.82%	21.80%	1.014	1.054	2.19 $^{+0.11}_{-0.11}$ ±0.11	2.08 $^{+0.11}_{-0.10}$ ±0.10
4.189	570.0	63.5 $^{+8.3}_{-8.3}$	21.3 $^{+5.2}_{-4.5}$	27.61%	21.93%	1.017	1.056	2.52 $^{+0.29}_{-0.28}$ ±0.13	2.38 $^{+0.28}_{-0.27}$ ±0.12
4.199	526.0	36.0 $^{+6.4}_{-6.4}$	17.6 $^{+4.9}_{-4.1}$	27.92%	21.99%	1.020	1.056	1.70 $^{+0.26}_{-0.24}$ ±0.09	1.61 $^{+0.24}_{-0.23}$ ±0.08
4.209	572.0	46.5 $^{+7.3}_{-7.3}$	10.7 $^{+3.6}_{-2.9}$	27.45%	21.63%	1.021	1.057	1.70 $^{+0.24}_{-0.23}$ ±0.08	1.61 $^{+0.23}_{-0.22}$ ±0.08
4.219	569.2	48.0 $^{+7.1}_{-7.1}$	18.7 $^{+4.8}_{-4.1}$	27.43%	21.65%	1.024	1.056	1.98 $^{+0.26}_{-0.24}$ ±0.10	1.88 $^{+0.24}_{-0.23}$ ±0.09
4.226	1100.9	106.2 $^{+10.9}_{-10.9}$	53.6 $^{+7.6}_{-6.9}$	27.90%	22.14%	1.026	1.056	2.41 $^{+0.20}_{-0.19}$ ±0.12	2.28 $^{+0.19}_{-0.18}$ ±0.11
4.236	530.3	44.1 $^{+6.9}_{-6.9}$	17.0 $^{+4.5}_{-3.9}$	27.57%	21.99%	1.029	1.056	1.93 $^{+0.26}_{-0.25}$ ±0.10	1.82 $^{+0.25}_{-0.24}$ ±0.09
4.244	538.1	45.3 $^{+7.1}_{-7.1}$	18.5 $^{+4.6}_{-3.9}$	27.78%	22.04%	1.031	1.056	1.97 $^{+0.26}_{-0.25}$ ±0.10	1.86 $^{+0.25}_{-0.24}$ ±0.09
4.258	828.4	73.5 $^{+9.0}_{-9.0}$	25.1 $^{+6.1}_{-4.8}$	27.82%	22.04%	1.035	1.054	1.96 $^{+0.22}_{-0.20}$ ±0.10	1.86 $^{+0.21}_{-0.19}$ ±0.09
4.267	531.1	45.2 $^{+6.9}_{-6.9}$	23.4 $^{+5.5}_{-4.8}$	27.76%	21.95%	1.038	1.053	2.13 $^{+0.27}_{-0.26}$ ±0.11	2.02 $^{+0.26}_{-0.25}$ ±0.10
4.278	175.7	7.9 $^{+3.2}_{-2.6}$	4.9 $^{+2.5}_{-1.9}$	27.19%	21.48%	1.042	1.053	1.22 $^{+0.39}_{-0.31}$ ±0.06	1.16 $^{+0.37}_{-0.29}$ ±0.06
4.288	502.4	32.0 $^{+6.3}_{-6.3}$	15.6 $^{+4.2}_{-3.6}$	26.99%	21.29%	1.083	1.053	1.54 $^{+0.25}_{-0.24}$ ±0.08	1.46 $^{+0.23}_{-0.22}$ ±0.07
4.308	45.1	1.9 $^{+1.7}_{-1.0}$	1.0 $^{+1.3}_{-0.0}$	27.53%	21.83%	1.051	1.052	1.06 $^{+0.78}_{-0.36}$ ±0.05	1.00 $^{+0.74}_{-0.35}$ ±0.05
4.312	501.2	34.0 $^{+6.1}_{-6.1}$	12.7 $^{+4.0}_{-3.4}$	27.08%	21.06%	1.087	1.052	1.51 $^{+0.24}_{-0.23}$ ±0.08	1.44 $^{+0.22}_{-0.22}$ ±0.07
4.337	505.0	27.1 $^{+5.6}_{-5.6}$	12.7 $^{+3.8}_{-3.2}$	26.98%	21.27%	1.093	1.051	1.27 $^{+0.22}_{-0.21}$ ±0.06	1.21 $^{+0.21}_{-0.20}$ ±0.06
4.358	543.9	52.7 $^{+7.4}_{-7.4}$	12.5 $^{+4.1}_{-3.4}$	27.69%	21.65%	1.065	1.051	1.94 $^{+0.25}_{-0.24}$ ±0.10	1.85 $^{+0.24}_{-0.23}$ ±0.09
4.377	522.7	24.7 $^{+5.3}_{-5.3}$	17.6 $^{+4.4}_{-3.9}$	26.92%	21.13%	1.102	1.051	1.30 $^{+0.21}_{-0.20}$ ±0.07	1.24 $^{+0.20}_{-0.19}$ ±0.06
4.396	507.8	37.5 $^{+6.3}_{-6.3}$	10.6 $^{+3.8}_{-3.2}$	26.80%	20.86%	1.106	1.051	1.53 $^{+0.23}_{-0.22}$ ±0.08	1.45 $^{+0.22}_{-0.21}$ ±0.07
4.416	1090.7	83.3 $^{+9.4}_{-9.4}$	24.4 $^{+5.2}_{-4.6}$	27.14%	21.32%	1.082	1.052	1.60 $^{+0.16}_{-0.16}$ ±0.08	1.52 $^{+0.15}_{-0.15}$ ±0.08
4.436	569.9	47.0 $^{+7.5}_{-7.5}$	14.4 $^{+4.3}_{-3.6}$	26.65%	21.00%	1.116	1.054	1.72 $^{+0.24}_{-0.23}$ ±0.09	1.64 $^{+0.23}_{-0.22}$ ±0.08
4.467	111.1	4.8 $^{+2.5}_{-1.9}$	1.0 $^{+1.3}_{-0.7}$	26.94%	20.93%	1.096	1.055	0.85 $^{+0.41}_{-0.30}$ ±0.04	0.80 $^{+0.39}_{-0.28}$ ±0.04
4.527	112.1	6.6 $^{+2.8}_{-2.2}$	2.9 $^{+2.0}_{-1.4}$	26.64%	20.61%	1.112	1.054	1.37 $^{+0.50}_{-0.38}$ ±0.07	1.30 $^{+0.47}_{-0.36}$ ±0.06
4.600	586.9	24.0 $^{+4.9}_{-4.9}$	14.6 $^{+4.1}_{-3.5}$	26.40%	20.54%	1.132	1.055	1.05 $^{+0.17}_{-0.16}$ ±0.05	1.00 $^{+0.17}_{-0.16}$ ±0.05
4.612	103.8	4.9 $^{+2.5}_{-1.9}$	0.0 $^{+0.5}_{-0.0}$	26.01%	19.95%	1.158	1.055	0.75 $^{+0.39}_{-0.29}$ ±0.04	0.71 $^{+0.37}_{-0.28}$ ±0.04
4.628	521.5	28.5 $^{+5.6}_{-5.6}$	8.7 $^{+3.5}_{-2.8}$	25.85%	19.76%	1.162	1.054	1.14 $^{+0.20}_{-0.19}$ ±0.06	1.08 $^{+0.19}_{-0.18}$ ±0.05
4.641	552.4	27.5 $^{+5.4}_{-5.4}$	8.8 $^{+3.6}_{-2.9}$	25.90%	19.74%	1.164	1.054	1.05 $^{+0.19}_{-0.18}$ ±0.05	0.99 $^{+0.18}_{-0.17}$ ±0.05
4.661	529.6	27.6 $^{+5.1}_{-5.1}$	17.5 $^{+4.4}_{-3.8}$	25.59%	19.59%	1.169	1.054	1.37 $^{+0.20}_{-0.19}$ ±0.07	1.30 $^{+0.19}_{-0.18}$ ±0.06
4.682	1669.3	66.4 $^{+8.5}_{-8.5}$	21.2 $^{+5.3}_{-4.4}$	25.69%	19.53%	1.174	1.054	0.84 $^{+0.10}_{-0.09}$ ±0.04	0.79 $^{+0.09}_{-0.09}$ ±0.04
4.699	536.5	16.7 $^{+4.3}_{-4.3}$	8.5 $^{+3.3}_{-2.7}$	25.76%	19.25%	1.178	1.055	0.75 $^{+0.16}_{-0.15}$ ±0.04	0.71 $^{+0.15}_{-0.14}$ ±0.04
4.740	164.3	11.3 $^{+3.4}_{-3.4}$	2.9 $^{+2.0}_{-1.4}$	26.18%	19.52%	1.188	1.055	1.35 $^{+0.37}_{-0.35}$ ±0.07	1.28 $^{+0.35}_{-0.33}$ ±0.06
4.750	367.2	8.9 $^{+3.6}_{-3.0}$	8.8 $^{+3.3}_{-2.6}$	26.23%	19.61%	1.192	1.055	0.75 $^{+0.21}_{-0.17}$ ±0.04	0.71 $^{+0.20}_{-0.16}$ ±0.04
4.781	512.8	20.2 $^{+4.7}_{-4.7}$	11.7 $^{+3.7}_{-3.1}$	25.82%	19.57%	1.199	1.055	0.97 $^{+0.18}_{-0.17}$ ±0.05	0.92 $^{+0.17}_{-0.16}$ ±0.05
4.843	527.3	25.7 $^{+5.3}_{-5.3}$	7.5 $^{+3.2}_{-2.5}$	25.63%	19.13%	1.213	1.056	0.98 $^{+0.18}_{-0.17}$ ±0.05	0.93 $^{+0.17}_{-0.16}$ ±0.05
4.918	208.1	9.4 $^{+3.3}_{-2.7}$	1.9 $^{+1.7}_{-1.1}$	25.04%	18.94%	1.234	1.056	0.85 $^{+0.28}_{-0.22}$ ±0.04	0.80 $^{+0.26}_{-0.21}$ ±0.04
4.951	160.4	6.4 $^{+2.8}_{-2.2}$	4.9 $^{+2.8}_{-2.2}$	24.78%	18.49%	1.244	1.056	1.11 $^{+0.39}_{-0.30}$ ±0.06	1.05 $^{+0.37}_{-0.29}$ ±0.05



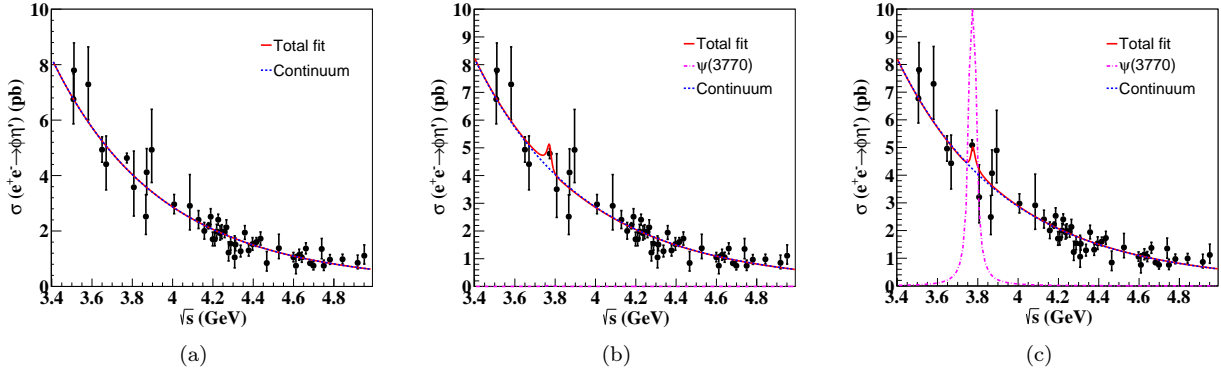


Fig. 3. Dressed cross sections of the  $e^+e^- \rightarrow \phi\eta'$  process and the fits under different assumptions: (a) continuum amplitude only; (b) coherent sum of continuum and  $\psi(3770)$  amplitudes, the solution with  $\Phi = 2.0$  rad,  $\mathcal{B}_{\phi\eta'} = 4.6 \times 10^{-6}$ , and the significance of the  $\psi(3770) \rightarrow \phi\eta'$  decay is  $1.5\sigma$ ; (c) coherent sum of continuum and  $\psi(3770)$  amplitudes, the solution with  $\Phi = 4.7$  rad,  $\mathcal{B}_{\phi\eta'} = 1.9 \times 10^{-3}$ , and the significance of the  $\psi(3770) \rightarrow \phi\eta'$  decay is  $1.6\sigma$ . The black dots with error bars are data. The red solid lines are the total fits, the magenta dot dashed lines represent the  $\psi(3770)$  component, and the blue dashed lines the continuum process.

given by

$$\chi^2 = \sum_j \frac{(\sigma_j - \sigma_j^{\text{fit}})^2}{\delta_j^2}, \quad (4)$$

where  $\sigma_j$ ,  $\sigma_j^{\text{fit}}$ , and  $\delta_j$  are the measured dressed cross section, the fitted cross section, and the statistical uncertainty of the measured cross section of the  $j$ th energy point, respectively.

The cross sections are described with a coherent sum of the continuum and the  $\psi(3770)$  amplitudes

$$\sigma^{\text{dressed}}(\sqrt{s}) = \left| \frac{a}{(\sqrt{s})^n} \sqrt{\text{PS}(\sqrt{s})} + e^{i\Phi} \text{BW}(\sqrt{s}) \right|^2, \quad (5)$$

where the constants  $a$  and  $n$  describe the magnitude and slope of the continuum process,  $\Phi$  is the relative phase between the continuum and the  $\psi(3770)$  amplitudes,  $\text{PS}(\sqrt{s}) = q^3(\sqrt{s})/s$  is the P-wave phase space factor [23], and  $q(\sqrt{s})$  is the momentum of  $\phi$  and  $\eta'$  in the  $e^+e^-$  c.m. frame.

The  $\psi(3770)$  resonance is parameterized with a Breit-Wigner (BW) function

$$\text{BW}(\sqrt{s}) = \frac{\sqrt{12\pi\Gamma_{e^+e^-}\Gamma_{\text{tot}}\mathcal{B}_{\phi\eta'}}}{s - M^2 + iM\Gamma_{\text{tot}}} \sqrt{\frac{\text{PS}(\sqrt{s})}{\text{PS}(M)}}, \quad (6)$$

where  $M$ ,  $\Gamma_{\text{tot}}$ , and  $\Gamma_{e^+e^-}$  are the mass, width, and electronic partial width of  $\psi(3770)$ , and all of them are set to their PDG values [23].  $\mathcal{B}_{\phi\eta'}$  is the branching fraction of  $\psi(3770) \rightarrow \phi\eta'$ .

For the data samples far from  $\sqrt{s} = 3.773$  GeV, the interference between the  $\psi(3770)$  and continuum amplitudes can be ignored. Without the data sample at  $\sqrt{s} = 3.773$  GeV, the pure continuum process ( $\sigma^{\text{dressed}}(\sqrt{s}) =$

$|\frac{a}{(\sqrt{s})^n} \sqrt{\text{PS}(\sqrt{s})}|^2$ ) is used to fit the dressed cross sections. From this fit,  $a = 1.97 \pm 0.40$  ( $\text{GeV}^{n-0.5} \text{pb}^{0.5}$ ) and  $n = 4.35 \pm 0.14$  are obtained, where the uncertainties are statistical only. The systematic uncertainties of the cross section measurements (see below) have negligible effect on  $n$ . The fit result is shown in Fig. 3(a).

Due to the lack of high integrated luminosity data in the vicinity of the  $\psi(3770)$ , the fit including the  $\sqrt{s} = 3.773$  GeV data and the resonance contribution is not stable. A two-dimensional parameter scan of  $\mathcal{B}_{\phi\eta'}$  and  $\Phi$  is performed under all possible line shape assumptions. In the scan, the parameters  $a$  and  $n$  describing the continuum amplitudes are fixed to the central values obtained from the continuum-only fit. The resonance parameters of  $\psi(3770)$ ,  $M$ ,  $\Gamma_{\text{tot}}$ , and  $\Gamma_{e^+e^-}$  are fixed to the corresponding PDG values [23]. We scan  $\mathcal{B}_{\phi\eta'}$  and  $\Phi$  from 0 to  $2.3 \times 10^{-3}$  and from 0 to  $2\pi$  in steps of  $7.6 \times 10^{-6}$  and 0.02, respectively. Figure 4 shows the scanning result, where the color scale represents the value of  $\chi^2$  defined in Eq. (4). The  $i$ th  $\sigma$  contour is defined by  $\chi^2 = \chi_{\text{min}}^2 + i^2$  [48], where  $\chi_{\text{min}}^2$  is the minimal  $\chi^2$  value. The probability that both parameters simultaneously take values within the one standard deviation ( $1\sigma$ ) contour is 39.3%. The fit result corresponding to the minimum in the scan (shown in Fig. 4) is shown in Fig. 3(c). The parameters  $\mathcal{B}_{\phi\eta'}$  and  $\Phi$  corresponding to the minimum  $\chi^2$  value is  $(1.9 \times 10^{-3}, 4.7 \text{ rad})$ , and the corresponding  $\chi_{\text{min}}^2$  is 48.0, which is slightly smaller than the  $\chi^2$  of Fig. 3(b) ( $\chi^2 = 48.2$ ). Therefore, these two solutions correspond to different line shapes and do not originate from the multiple-solution problems discussed in Ref. [56]. The significance of the  $\psi(3770) \rightarrow \phi\eta'$  decay is less than  $2\sigma$  by comparing the fit  $\chi^2$ s ( $\Delta\chi^2 = 4.4$ ) with and without including the  $\psi(3770)$  amplitude and taking the change of the number of degrees of freedom ( $\Delta\text{ndf} = 2$ ) into account. For the fitted parameter of

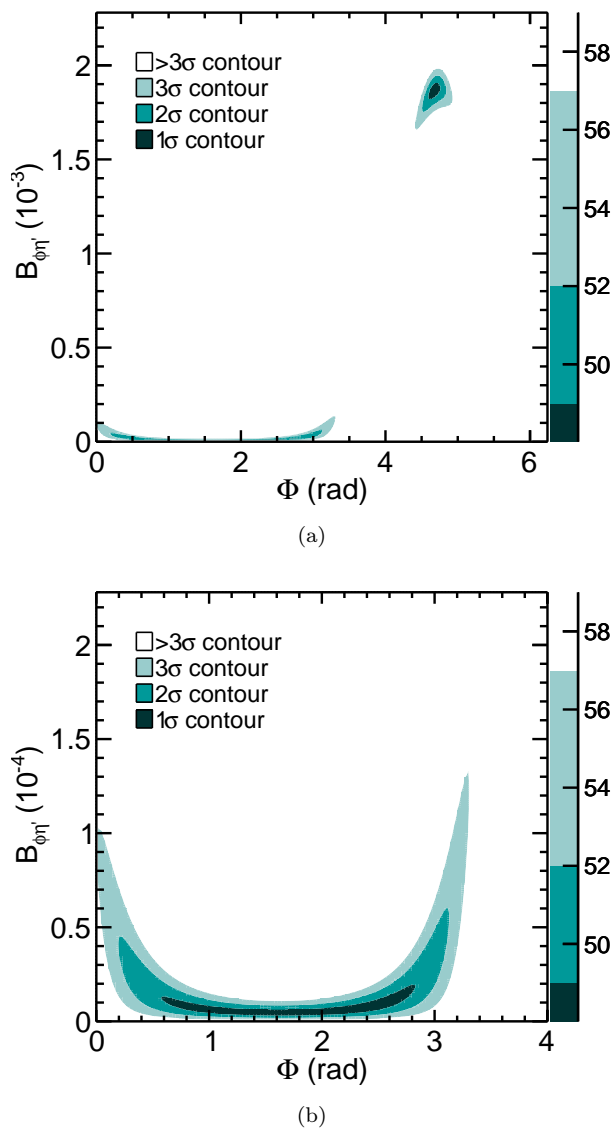


Fig. 4. The two-dimensional scan result of the parameters  $\mathcal{B}_{\phi\eta'}$  and  $\Phi$ . In (a), the  $y$ -axis is from 0 to  $2.3 \times 10^{-3}$ , and the upper right contour corresponds to Fig. 3(c) and the bottom contour corresponds to Fig. 3(b), respectively; in (b), the  $y$ -axis is from 0 to  $2.3 \times 10^{-4}$  (Plot (b) is the subset of plot (a)). The color in the figure represents the value of  $\chi^2$  in different  $\sigma$  intervals defined in Eq. (4).

$\mathcal{B}_{\phi\eta'} = 1.9 \times 10^{-3}$ , the cross section of  $\psi(3770) \rightarrow \phi\eta'$  is of the same order of magnitude as that of the continuum process, as shown in Fig. 3(c). Due to destructive interference, a small structure appears above the expectation of the continuum process, which has also been observed in  $e^+e^- \rightarrow \Lambda\bar{\Lambda}$ ,  $\omega\pi^0$  and  $\omega\eta$  processes [31, 57, 58]. Considering the fact that the cross section of  $\psi(3770) \rightarrow$  light hadrons is much smaller than the continuum production of  $e^+e^- \rightarrow$  light hadrons, we exclude the non-physical solution where the cross section is compatible to the continuum production. The physical solution, which lies within the  $1\sigma$  contour range of  $\mathcal{B}_{\phi\eta'} \in [0.3, 1.9] \times 10^{-5}$

and  $\Phi \in [0.6, 2.8]$  rad, is shown in Fig. 4(b).

## V. SYSTEMATIC UNCERTAINTY

The systematic uncertainties of the cross section measurements are classified into two categories: correlated terms and uncorrelated terms. Correlated terms are common to the two  $\eta'$  decay modes, including the luminosity measurements, the differences between data and MC simulation for the tracking efficiency, photon reconstruction efficiency, the branching fraction of the  $\phi$  decay, and the mass window for  $\phi$  candidate. Uncorrelated terms are different in each  $\eta'$  decay mode, including the branching fractions of  $\eta'$  and  $\eta$  decays, the  $\eta$  reconstruction efficiency, the 4C/5C kinematic fits, the mass window for  $\eta'$  candidate, the signal shape and the background shape. These two categories of uncertainties are discussed in detail below.

The integrated luminosities of the data samples used in this study are measured using large angle Bhabha scattering events, with an uncertainty ranging within (0.5–1)% [53–55]. We conservatively take 1% as the corresponding systematic uncertainty. The uncertainty of the difference in the tracking efficiencies between data and MC simulations is estimated to be 1% per track [59, 60]. The uncertainty of the photon reconstruction efficiency is determined through dedicated studies [61, 62] and is found to be 1% per photon. The uncertainties related to the branching fractions of  $\phi \rightarrow K^+K^-$ ,  $\eta' \rightarrow \gamma\pi^+\pi^-$ ,  $\eta' \rightarrow \eta\pi^+\pi^-$ , and  $\eta \rightarrow \gamma\gamma$  are taken from PDG [23]. The uncertainty caused by the  $\eta$  reconstruction is determined by using a high purity control sample of  $J/\psi \rightarrow \eta p\bar{p}$  decays [63]. The study utilized the  $\eta$  yields revealed in the  $\gamma\gamma$  mass spectrum with or without  $\eta$  selection requirements to determine the  $\eta$  reconstruction efficiency. Given the negligible statistical error of the test sample, the observed 1% difference of the  $\eta$  reconstruction efficiencies between data and MC simulations is taken as the systematic uncertainty.

To address the uncertainty caused by the 4C/5C kinematic fit, we adjust the track helix parameters of charged tracks in the MC simulation so that it better describes the momentum spectra of the data [64]. In this study, we utilize the efficiency after the helix correction to obtain the nominal results. The difference in the MC efficiencies before and after the correction is taken as the systematic uncertainty.

The efficiencies obtained from MC simulation are corrected according to the data-MC difference in efficiencies obtained with the control sample of  $\psi(2S) \rightarrow \phi\eta'$  decays. The correction factor  $f^v$  is defined as

$$f^v = \varepsilon_{\text{MC}}^v / \varepsilon_{\text{data}}^v, \quad (7)$$

with

$$\varepsilon_{\text{data(MC)}}^v = N_{\text{data(MC)}}^v / M_{\text{data(MC)}}^v, \quad (8)$$

where the subscripts "MC" and "data" represent MC and data samples, respectively,  $N_{\text{data(MC)}}^v$  is the number of events in the signal region of a selection criterion  $v$ , and  $M_{\text{data(MC)}}^v$  is the number of events in the full range of  $v$ . The relative uncertainty of the correction factor  $f^v$  is calculated as a quadratic sum of the relative statistical errors of  $\varepsilon_{\text{data}}^v$  and  $\varepsilon_{\text{MC}}^v$ .

A correction will not be applied if the correction factor  $f^v$  differs from unity by less than its uncertainty; otherwise the MC efficiency will be corrected as  $\varepsilon = \varepsilon/f^v$ , and  $\sigma_{f^v}$  will be taken as the systematic uncertainty. The systematic uncertainties due to the  $\phi$  and  $\eta'$  mass windows are estimated using the control sample of  $\psi(2S) \rightarrow \phi\eta'$  (with  $\eta' \rightarrow \gamma\pi^+\pi^-$  and  $\eta' \rightarrow \eta\pi^+\pi^-$  ( $\eta \rightarrow \gamma\gamma$ ) for modes I and II, respectively). The correction factors  $f^v$  are  $1.0072 \pm 0.0019$  for the  $\phi$  mass window, and  $1.0065 \pm 0.0032$  (mode I) and  $1.0104 \pm 0.0045$  (mode II) for the  $\eta'$  mass window.

For mode I, the parameters of the Gaussian functions convolved with the signal MC shape to describe the data are fixed at those obtained at  $\sqrt{s} = 3.670, 3.867, 3.871, 4.278, 4.308, 4.467, 4.527, 4.699, 4.740, 4.918$  and  $4.951$  GeV. We vary the nominal mean and standard deviation of the Gaussian function by  $\pm 1\sigma$ , and the maximum difference in the signal yields resulting from the various Gaussian function parameters is used to estimate the systematic uncertainty caused by the signal shape. We weight the systematic uncertainty of the signal shape by the luminosity of the data samples and obtain an estimated uncertainty of 1.6%. For mode II, because the background is relatively small, the Gaussian function parameters in all data samples are free in the fit, and there is no systematic uncertainty caused by the signal shape. The uncertainty associated with the background shape is estimated by changing from a first-order Chebyshev polynomial to a second-order one. To avoid any influence from statistical uncertainty, high statistical data samples at  $\sqrt{s} = 3.773, 4.178, 4.420, \text{ and } 4.680$  GeV are used to evaluate the systematic uncertainty caused by the parameterization of the background shape. The largest differences in the signal yields between different parameterizations of the background shape are taken as the systematic uncertainties, which are 1.4% and 2.7% for modes I and II, respectively.

Due to correlations between the two modes, the combined  $i$ th item of the systematic uncertainty  $\xi^i$  is calculated with

$$\xi^i = \frac{\sqrt{(w_{\text{I}}\xi_{\text{I}}^i)^2 + (w_{\text{II}}\xi_{\text{II}}^i)^2 + 2w_{\text{I}}w_{\text{II}}\rho_{\text{I,II}}\xi_{\text{I}}^i\xi_{\text{II}}^i}}{w_{\text{I}} + w_{\text{II}}}, \quad (9)$$

where  $w_{\text{I}} = \mathcal{B}(\eta' \rightarrow \gamma\pi^+\pi^-) \cdot \epsilon_1$ , and  $w_{\text{II}} = \mathcal{B}(\eta' \rightarrow \eta\pi^+\pi^-) \cdot \mathcal{B}(\eta \rightarrow \gamma\gamma) \cdot \epsilon_2$ . Here,  $\xi_{\text{I}}^i$  and  $\xi_{\text{II}}^i$  are the systematic uncertainties for modes I and II listed in Table II, respectively, and  $\rho_{\text{I,II}}$  is the correlation coefficient between modes I and II. For the systematic uncertainties caused by the luminosity measurements, the tracking efficiency,

the photon reconstruction efficiency, the branching fraction of the  $\phi$  decay, and the mass window for  $\phi$  candidate,  $\rho_{\text{I,II}}$  is taken as 1, for the other sources as 0.

Table II. The systematic uncertainties for the cross section measurements.

Source	Systematic uncertainty (%)		
	$\eta' \rightarrow \gamma\pi^+\pi^-$	$\eta' \rightarrow \eta\pi^+\pi^-$	Combination
Luminosity	1.0	1.0	1.0
Tracking	4.0	4.0	4.0
Photon	1.0	2.0	1.3
$\mathcal{B}(\phi \rightarrow K^+K^-)$	1.0	1.0	1.0
$\mathcal{B}(\eta' \rightarrow \gamma\pi^+\pi^-)$	1.4	-	1.0
$\mathcal{B}(\eta' \rightarrow \eta\pi^+\pi^-)$	-	1.2	0.4
$\mathcal{B}(\eta \rightarrow \gamma\gamma)$	-	0.5	0.2
$\eta$ reconstruction	-	1.0	0.3
Kinematic fit	1.2	0.7	0.9
Mass window of $\phi$	0.2	0.2	0.2
Mass window of $\eta'$	0.3	0.5	0.3
Signal shape	1.6	-	1.1
Background shape	1.4	2.7	1.3
Total	5.2	5.7	5.0

Table II summarizes all the systematic uncertainties related to the cross section measurements for the individual decay modes and the combined one. The overall multiplicative systematic uncertainties are obtained by adding all systematic uncertainties in quadrature assuming they are independent.

## VI. UPPER LIMIT ON THE BRANCHING FRACTION OF $\psi(3770) \rightarrow \phi\eta'$

There is no obvious structure in the dressed cross sections of  $e^+e^- \rightarrow \phi\eta'$ , as shown in Fig. 3. Based on the Bayesian method [65], the upper limit of the  $\mathcal{B}_{\phi\eta'}$  at the 90% confidence level (C.L.) is calculated with the systematic uncertainty taken into account. The least-chi-square fits are performed on the dressed cross sections of  $e^+e^- \rightarrow \phi\eta'$ , and the fitting estimator  $Q^2$  is constructed as

$$Q^2 = \sum_j \frac{(\sigma_j - \sigma_j^{\text{fit}})^2}{\zeta_j^2}, \quad (10)$$

where  $\sigma_j$ , and  $\sigma_j^{\text{fit}}$  are defined according to Eq. (4), and  $\zeta_j$  includes the statistical uncertainty and uncorrelated systematic uncertainty of the measured cross sections, which are summed in quadrature assuming they are independent.

We vary the parameters  $\mathcal{B}_{\phi\eta'}$  to get the distribution of  $Q^2$ . Then the likelihood distribution ( $L'$ ) as a function of the parameters  $\mathcal{B}_{\phi\eta'}$  is constructed as  $L'(\mathcal{B}_{\phi\eta'}) = e^{-0.5Q^2}$ . The normalized likelihood distribution is smeared with a Gaussian function, with a mean  $\varepsilon_0$  and a standard deviation  $\delta_\varepsilon = \varepsilon \times \delta_{\text{sys}}^{\text{cor}}$ , where  $\delta_\varepsilon$  and  $\delta_{\text{sys}}^{\text{cor}}$  are the absolute and

relative correlated systematic uncertainties, respectively. The normalized likelihood is defined as

$$L(\mathcal{B}_{\phi\eta'}) = \int_0^1 L'\left(\frac{\varepsilon}{\varepsilon_0} \cdot \mathcal{B}_{\phi\eta'}\right) \cdot \frac{1}{\sqrt{2\pi}\delta_\varepsilon} e^{-\frac{(\varepsilon-\varepsilon_0)^2}{2\delta_\varepsilon^2}} d\varepsilon, \quad (11)$$

where  $\varepsilon_0$  is the efficiency obtained from the MC simulation.

The parameters  $\mathcal{B}_{\phi\eta'}$  at the 90% C.L. ( $\mathcal{B}_{\phi\eta'}^{\text{up}}$ ) are determined as

$$\int_0^{\mathcal{B}_{\phi\eta'}^{\text{up}}} L(\mathcal{B}_{\phi\eta'}) d\mathcal{B}_{\phi\eta'} = 0.9 \int_0^\infty L(\mathcal{B}_{\phi\eta'}) d\mathcal{B}_{\phi\eta'}. \quad (12)$$

Considering the effect on the upper limit from the uncertainties of the mass and width measurements, we vary the nominal mass and width by  $\pm 1\sigma$  and choose the largest upper limit of  $\mathcal{B}_{\phi\eta'}$  among these combinations. The maximum of  $\mathcal{B}_{\phi\eta'}$  is near  $\Phi = 2.81$  rad within the  $1\sigma$  contour shown in Fig. 4. In order to obtain more conservative upper limits, the phase  $\Phi$  is fixed to 2.81 rad when determining the upper limit of  $\mathcal{B}_{\phi\eta'}$ . The normalized likelihood distribution is displayed in Fig. 5, and an upper limit of  $2.3 \times 10^{-5}$  is obtained for  $\mathcal{B}_{\phi\eta'}$  for the charmless decay of  $\psi(3770) \rightarrow \phi\eta'$ .

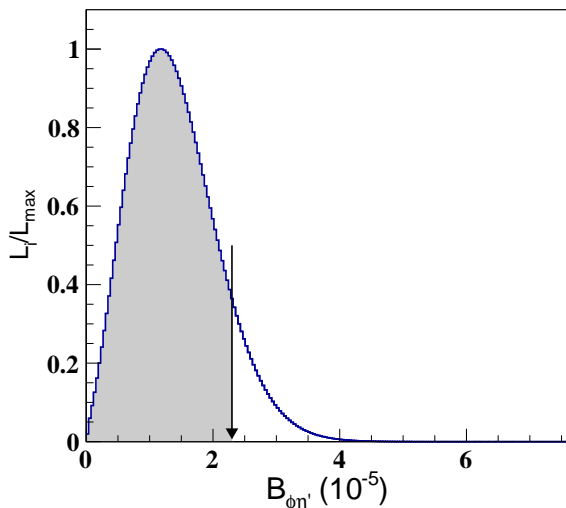


Fig. 5. The distribution of the likelihood versus  $\mathcal{B}_{\phi\eta'}$ , with the phase  $\Phi$  fixed to 2.81 rad. The black arrow shows the result corresponding to the 90% C.L.

## VII. SUMMARY AND DISCUSSIONS

The measurement of the  $e^+e^- \rightarrow \phi\eta'$  cross sections at center-of-mass energies from 3.508 to 4.951 GeV have been reported. The results in Table I show that the cross sections range from  $0.71 \pm 0.20$  to  $7.46 \pm 0.95$  pb, which is not consistent with  $\sim 60$  pb predicted by the NJL

model [7]. The power parameter,  $n = 4.35 \pm 0.14$ , is obtained from the fit to the cross sections. This value is in good agreement with the prediction of the NJL model ( $n = 3.5 \pm 0.9$ ) [7], where the uncertainty is solely systematic. However, it should be noted that the accuracy of the NJL model is (20-30)% for the calculation of the cross sections of the  $e^+e^- \rightarrow VP$  process. Our present study can therefore offer valuable insights to advance the development of the NJL model and enhance its precision in calculating the cross sections of the VP process.

By fitting the measured cross sections, we have also searched for the charmless decay  $\psi(3770) \rightarrow \phi\eta'$  and found that its statistical significance is less than  $2\sigma$ . The upper limit for the parameters  $\mathcal{B}_{\phi\eta'}$  of the  $\psi(3770)$  line shape has been determined to be  $2.3 \times 10^{-5}$ , which is in agreement with the model prediction of  $(0.5 - 3.5) \times 10^{-5}$  [29, 30]. This suggests that the S- and D-wave charmonium states mixing scheme may play a role in explaining the “ $\rho\pi$  puzzle” in  $J/\psi$ ,  $\psi(2S)$ , and  $\psi(3770)$  charmless decays. This study, together with previous searches for exclusive  $\psi(3770)$  charmless decays, provides valuable insights into the nature of the  $\psi(3770)$ , but the large  $\psi(3770)$  non- $D\bar{D}$  decay rate remains a puzzle. In the future, a fine energy scan of the  $\psi(3770)$  resonance would be necessary to determine the presence and magnitude of its charmless decays.

## VIII. ACKNOWLEDGMENT

The BESIII Collaboration thanks the staff of BEPCII and the IHEP computing center for their strong support. This work is supported in part by National Key R&D Program of China under Contracts Nos. 2020YFA0406300, 2020YFA0406400; National Natural Science Foundation of China (NSFC) under Contracts Nos. 11635010, 11735014, 11835012, 11935015, 11935016, 11935018, 11961141012, 12022510, 12025502, 12035009, 12035013, 12061131003, 12192260, 12192261, 12192262, 12192263, 12192264, 12192265, 12221005, 12225509, 12235017; the Chinese Academy of Sciences (CAS) Large-Scale Scientific Facility Program; the CAS Center for Excellence in Particle Physics (CCEPP); Joint Large-Scale Scientific Facility Funds of the NSFC and CAS under Contract No. U1832207; CAS Key Research Program of Frontier Sciences under Contracts Nos. QYZDJ-SSW-SLH003, QYZDJ-SSW-SLH040; 100 Talents Program of CAS; The Institute of Nuclear and Particle Physics (INPAC) and Shanghai Key Laboratory for Particle Physics and Cosmology; ERC under Contract No. 758462; European Union’s Horizon 2020 research and innovation programme under Marie Skłodowska-Curie grant agreement under Contract No. 894790; German Research Foundation DFG under Contracts Nos. 455635585, Collaborative Research Center CRC 1044, FOR5327, GRK 2149; Istituto Nazionale di Fisica Nucleare, Italy; Ministry of Development of

Turkey under Contract No. DPT2006K-120470; National Research Foundation of Korea under Contract No. NRF-2022R1A2C1092335; National Science and Technology fund of Mongolia; National Science Research and Innovation Fund (NSRF) via the Program Management

Unit for Human Resources & Institutional Development, Research and Innovation of Thailand under Contract No. B16F640076; Polish National Science Centre under Contract No. 2019/35/O/ST2/02907; The Swedish Research Council; U. S. Department of Energy under Contract No. DE-FG02-05ER41374.

- 
- [1] M. Davier, *Ann. Rev. Nucl. Part. Sci.* **63**, 407 (2013).  
 [2] Y. Nambu and G. Jona-Lasinio, *Phys. Rev.* **122**, 345 (1961).  
 [3] M. K. Volkov, *Sov. J. Part. Nucl.* **17**, 186 (1986).  
 [4] M. K. Volkov and A. E. Radzhabov, *Phys. Usp.* **49**, 551 (2006).  
 [5] J. Prades, *Z. Phys. C* **63**, 491 (1994); **11**, 571(E) (1999).  
 [6] B. Aubert *et al.* (BABAR Collaboration), *Phys. Rev. D* **76**, 092005 (2007).  
 [7] Y. M. Bystritskiy, E. A. Kuraev, M. Secansky and M. K. Volkov, *Int. J. Mod. Phys. A* **24**, 2629 (2009), arxiv:0804.3714v4 [hep-ph].  
 [8] P. A. Rapidis *et al.* (MARKI Collaboration), *Phys. Rev. Lett.* **39**, 526 (1977).  
 [9] E. Eichten, K. Gottfried, T. Kinoshita, J. B. Kogut, K. D. Lane and T. M. Yan, *Phys. Rev. Lett.* **34**, 369 (1975).  
 [10] E. Eichten, K. Gottfried, T. Kinoshita, K. D. Lane and T. M. Yan, *Phys. Rev. D* **21**, 203 (1980).  
 [11] M. Ablikim *et al.* (BES Collaboration), *Phys. Rev. Lett.* **97**, 121801 (2006).  
 [12] M. Ablikim *et al.* (BES Collaboration), *Phys. Lett. B* **641**, 145 (2006).  
 [13] M. Ablikim *et al.* (BES Collaboration), *Phys. Rev. D* **76**, 122002 (2007).  
 [14] M. Ablikim *et al.* (BES Collaboration), *Phys. Lett. B* **659**, 74 (2008).  
 [15] D. Besson *et al.* (CLEO Collaboration), *Phys. Rev. Lett.* **96**, 092002 (2006).  
 [16] J. Z. Bai *et al.* (BES Collaboration), *HEP & NP* **28**, 325 (2004).  
 [17] J. Z. Bai *et al.* (BES Collaboration), *Phys. Lett. B* **605**, 63 (2005).  
 [18] N. E. Adam *et al.* (CLEO Collaboration), *Phys. Rev. Lett.* **96**, 082004 (2006).  
 [19] B. A. Briere *et al.* (CLEO Collaboration), *Phys. Rev. D* **74**, 031106 (2006).  
 [20] T. E. Coans *et al.* (CLEO Collaboration), *Phys. Rev. Lett.* **96**, 182002 (2006).  
 [21] G. S. Adams *et al.* (CLEO Collaboration), *Phys. Rev. D* **73**, 012002 (2006).  
 [22] G. S. Huang *et al.* (CLEO Collaboration), *Phys. Rev. Lett.* **96**, 032003 (2006).  
 [23] R. L. Workman *et al.* (Particle Data Group), *PTEP* **2022**, 083C01 (2022).  
 [24] M. Ablikim *et al.* (BESIII Collaboration), *Phys. Rev. Lett.* **127**, 082002 (2021).  
 [25] E. Eichten, K. Gottfried, T. Kinoshita, K. D. Lane and T. M. Yan, *Phys. Rev. D* **17**, 3090 (1978).  
 [26] Y. P. Kuang and T. M. Yan, *Phys. Rev. D* **41**, 155 (1990).  
 [27] T. Appelquist and H. D. Politzer, *Phys. Rev. Lett.* **34**, 43 (1975).  
 [28] A. De Rújula and S. L. Glashow, *Phys. Rev. Lett.* **34**, 46 (1975).  
 [29] P. Wang, C. Z. Yuan and X. H. Mo, *Phys. Lett. B* **574**, 41 (2003).  
 [30] P. Wang, X. H. Mo and C. Z. Yuan, *Phys. Rev. D* **70**, 077505 (2004).  
 [31] M. Ablikim *et al.* (BESIII Collaboration), *Phys. Rev. D* **107**, 072003 (2023).  
 [32] M. Ablikim *et al.* (BESIII Collaboration), *Nucl. Instrum. Meth. A* **614**, 345 (2010).  
 [33] C. H. Yu *et al.*, Proceedings of IPAC2016, Busan, Korea, 2016.  
 [34] K. X. Huang *et al.*, *Nucl. Sci. Tech.* **33**, 142 (2022).  
 [35] X. Li *et al.*, *Radiat. Detect. Technol. Methods* **1**, 13 (2017).  
 [36] Y. X. Guo *et al.*, *Radiat. Detect. Technol. Methods* **1**, 15 (2017).  
 [37] S. Agostinelli *et al.* (GEANT4 Collaboration), *Nucl. Instrum. Meth. A* **506**, 250 (2003).  
 [38] Z. Y. Deng *et al.*, *Chin. Phys. C* **30**, 371 (2006).  
 [39] S. Jadach, B. F. L. Ward and Z. Wąs, *Comput. Phys. Commun.* **130**, 260 (2000).  
 [40] S. Jadach, B. F. L. Ward and Z. Wąs, *Phys. Rev. D* **63**, 113009 (2001).  
 [41] D. J. Lange, *Nucl. Instrum. Meth. A* **462**, 152 (2001).  
 [42] R. G. Ping, *Chin. Phys. C* **32**, 599 (2008).  
 [43] N. Qin, Z. Y. Zhang, S. S. Fang, X. Zhou, L. L. Du and H. X. Qiao, *Chin. Phys. C* **42** 013001, (2018).  
 [44] E. Richter-Was, *Phys. Lett. B* **303**, 163 (1993).  
 [45] G. Balossini, C. M. Carloni Calame, G. Montagna, O. Nicrosini and F. Piccinini, *Nucl. Phys. B* **758**, 227 (2006).  
 [46] J. C. Chen, G. S. Huang, X. R. Qi, D. H. Zhang and Y. S. Zhu, *Phys. Rev. D* **62**, 034003 (2000).  
 [47] R. L. Yang, R. G. Ping and H. Chen, *Chin. Phys. Lett.* **31**, 061301 (2014).  
 [48] W. T. Eadie, D. Drijard, F. James, M. Roos, and B. Sadoulet, *Journal of the American Statistical Association* **68**, 494 (1973).  
 [49] S. Actis *et al.*, *Eur. Phys. J. C* **66**, 585 (2010).  
 [50] E. A. Kuraev and V. S. Fadin, *Sov. J. Nucl. Phys.* **41**, 466 (1985).  
 [51] W. Y. Sun, T. Liu, M. Q. Jing, L. L. Wang, B. Zhong and W. M. Song, *Front. Phys.* **16**, 64501 (2021).  
 [52] M. Ablikim *et al.* (BESIII Collaboration), *Chin. Phys. C* **40**, 063001 (2016).  
 [53] M. Ablikim *et al.* (BESIII Collaboration), *Chin. Phys. C* **39**, 093001 (2015).  
 [54] M. Ablikim *et al.* (BESIII Collaboration), *Chin. Phys. C* **46**, 113003 (2022).  
 [55] M. Ablikim *et al.* (BESIII Collaboration), *Chin. Phys. C* **46**, 113002 (2022).

- [56] K. Zhu, X. H. Mo, C. Z. Yuan and P. Wang, *Int. J. Mod. Phys. A* **26**, 4511 (2011).
- [57] M. Ablikim *et al.* (BESIII Collaboration), *Phys. Rev. D* **104**, L091104 (2021).
- [58] M. Ablikim *et al.* (BESIII Collaboration), *JHEP* **07**, 064 (2022).
- [59] M. Ablikim *et al.* (BESIII Collaboration), *Phys. Rev. D* **91**, 112004 (2015).
- [60] M. Ablikim *et al.* (BESIII Collaboration), *Phys. Rev. D* **99**, 031101 (2019).
- [61] M. Ablikim *et al.* (BESIII Collaboration), *Phys. Rev. D* **83**, 012006 (2011).
- [62] M. Ablikim *et al.* (BESIII Collaboration), *Phys. Rev. D* **83**, 032003 (2011).
- [63] M. Ablikim *et al.* (BESIII Collaboration), *Phys. Rev. Lett.* **105**, 261801 (2010).
- [64] M. Ablikim *et al.* (BESIII Collaboration), *Phys. Rev. D* **87**, 012002 (2013).
- [65] Y. S. Zhu, *Chin. Phys. C* **32**, 363 (2008).